

Rethinking the Ancient Sulfur Cycle

David A. Fike,^{1,*} Alexander S. Bradley,¹
and Catherine V. Rose²

¹Department of Earth and Planetary Sciences, Washington University, St. Louis, Missouri 63130; email: dfike@levee.wustl.edu, abradley@eps.wustl.edu

²Department of Geology, Trinity College Dublin, Dublin 2, Ireland; email: crose@tcd.ie

Annu. Rev. Earth Planet. Sci. 2015. 43:593–622

First published online as a Review in Advance on April 16, 2015

The *Annual Review of Earth and Planetary Sciences* is online at earth.annualreviews.org

This article's doi:
10.1146/annurev-earth-060313-054802

Copyright © 2015 by Annual Reviews.
All rights reserved

*Corresponding author

Keywords

sulfur isotopes, microbial sulfate reduction, carbonate-associated sulfate, pyrite, seawater sulfate

Abstract

The sulfur biogeochemical cycle integrates the metabolic activity of multiple microbial pathways (e.g., sulfate reduction, disproportionation, and sulfide oxidation) along with abiotic reactions and geological processes that cycle sulfur through various reservoirs. The sulfur cycle impacts the global carbon cycle and climate primarily through the remineralization of organic carbon. Over geological timescales, cycling of sulfur is closely tied to the redox state of Earth's exosphere through the burial of oxidized (sulfate) and reduced (sulfide) sulfur species in marine sediments. Biological sulfur cycling is associated with isotopic fractionations that can be used to trace the fluxes through various metabolic pathways. The resulting isotopic data provide insights into sulfur cycling in both modern and ancient environments via isotopic signatures in sedimentary sulfate and sulfide phases. Here, we review the deep-time $\delta^{34}\text{S}$ record of marine sulfates and sulfides in light of recent advances in understanding how isotopic signatures are generated by microbial activity, how these signatures are encoded in marine sediments, and how they may be altered following deposition. The resulting picture shows a sulfur cycle intimately coupled to ambient carbon cycling, where sulfur isotopic records preserved in sedimentary rocks are critically dependent on sedimentological and geochemical conditions (e.g., iron availability) during deposition.

Disproportionation:

metabolism in which an intermediate-valence species (e.g., elemental sulfur) is simultaneously reduced and oxidized to form different products (sulfate and H₂S)

Isotopic fractionation:

a difference in isotopic composition arising as the result of a physical, chemical, or biological process

Pyrite: iron sulfide mineral (FeS₂) that is the dominant sink of reduced sulfur from the ocean

δ³⁴S: stable isotopic composition of a sulfur phase, based on the ratio of ³⁴S to ³²S

INTRODUCTION

The biogeochemical sulfur cycle plays an important role in regulating Earth's surface conditions via the activity of a variety of microbial metabolic processes (e.g., sulfate reduction, disproportionation, and sulfide oxidation) that transform the oxidation state of sulfur. These metabolic activities are intimately linked to the global carbon cycle, particularly through the remineralization of organic carbon by sulfate reduction in marine sediments. Further, the long-term burial of oxidized (sulfate) relative to reduced (sulfide) minerals in marine sediments and sedimentary rocks regulates marine redox conditions and, ultimately, atmospheric oxygen levels (Berner & Raiswell 1983, Canfield 2001a, Garrels & Lerman 1981, Holland 1973). Through these couplings, the sulfur cycle is directly linked to the long-term evolution of Earth's oxidation state and climate. The diverse metabolic processes that constitute the sulfur cycle are associated with distinctive stable isotopic fractionations of sulfur species (Brunner & Bernasconi 2005; Canfield & Thamdrup 1994; Chambers et al. 1975; Fry et al. 1984; Habicht & Canfield 1997; Habicht et al. 1998; Johnston et al. 2005a; Kaplan & Rittenberg 1964; Leavitt et al. 2013a; Sim et al. 2011a,b). The distributions of the stable isotopes¹ of sulfur (³²S, ³³S, ³⁴S, and ³⁶S) among sulfur-bearing species can be used to trace the relative magnitude of various redox transformations. In modern environments, the isotopic compositions of aqueous sulfide and sulfate are used to constrain the presence and activity of different microbial pathways (Canfield 2001a,b; Canfield et al. 2010; Fike et al. 2008, 2009; Gomes & Hurtgen 2013; Nakagawa et al. 2012). In ancient geological deposits, the isotopic record of sulfur-bearing phases—predominantly sulfate minerals and sulfides, particularly pyrite (FeS₂)—can be used in a similar manner to reconstruct ocean chemistry at the time of deposition, thereby allowing researchers to infer the oxidation state of the ocean as it has evolved over Earth history (Canfield & Teske 1996, Claypool et al. 1980, Fike & Grotzinger 2008, Fike et al. 2006, Gill et al. 2007, Hurtgen et al. 2009, Johnston et al. 2005b, Jones & Fike 2013). The appearance of signatures relating to specific metabolic pathways can be further used to constrain the evolutionary appearance and importance of various metabolic pathways (Canfield & Teske 1996, Johnston et al. 2005b, Leavitt et al. 2013a, Philippot et al. 2007, Shen et al. 2001). The interpretation of these isotopic signatures requires careful attention to the types of metabolic processes capable of producing them, as well as to the physical, chemical, and biological processes that can affect their preservation, heterogeneity, and fidelity. Herein, we review the deep-time δ³⁴S² record of marine sulfates and sulfides in light of recent advances in understanding how isotopic signatures are generated by microbial activity, how these signatures are encoded in marine sediments, and how they may be altered following deposition.

BIOLOGICAL SULFUR CYCLING

Sulfur is an essential element for all living organisms, and assimilatory sulfur metabolism is ubiquitous among microorganisms, plants, and animals to construct biomolecules (e.g., the amino acids cysteine and methionine), coenzymes and cosubstrates, and inorganic components of biomolecules (e.g., the Fe-S complexes in electron transport enzymes). However, sulfur makes up less than one percent by weight of typical biomass (Canfield 2001a), and organic sulfur is generally thought to

¹Isotopic measurements can be made by examining any combination of the four stable isotopes of sulfur. Here we focus on the two most abundant isotopes (³²S and ³⁴S), which are by far the most frequently applied in both modern and ancient settings for the information they can provide to understand the sulfur cycle. Excellent discussions of additional information that can be gained from analysis of the minor isotopes (³³S and ³⁶S) are provided by Farquhar & Wing (2003) and Johnston (2011).

²δ³⁴S_{sample} = 1,000 × [(³⁴S/³²S)_{sample} / (³⁴S/³²S)_{standard} - 1], reported in permil (‰) relative to the Vienna Canyon Diablo Troilite (VCDT) standard.

play only a minor role in the biogeochemical sulfur cycle, although it can provide insights into the fate of organics during diagenesis (Amrani et al. 2006, Raven et al. 2015).

Dissimilatory microbial processes transform the oxidation state of sulfur for the purpose of energy conservation coupled to metabolism. A broad taxonomic spectrum of microbes can perform these transformations on a variety of organic and inorganic sulfur compounds. Three dissimilatory metabolic processes are particularly significant for the biogeochemical sulfur cycle: sulfate reduction, sulfide oxidation, and sulfur disproportionation. Reduced sulfur compounds such as hydrogen sulfide, sulfur, and thiosulfate can also serve as electron donors for photosynthesis, and thus for carbon fixation (Bryant & Frigaard 2006).

In marine and lacustrine sediments, the differing sulfur metabolic processes are often spatially segregated in response to the supply of oxidized and reduced compounds. In modern marine sediments, electrons are supplied directly or indirectly by organic material derived from primary producers. The oxidation of these compounds is coupled to the reduction of electron acceptors such as oxygen, nitrate, Fe^{3+} , Mn^{4+} , sulfate, and even CO_2 . The spatial ordering of electron acceptor consumption and the rates at which this occurs in redox-stratified sediment columns depend on the genetic capacity of the native microbial communities, the kinetics of each metabolic pathway, and the thermodynamic yield of the reactions. The more thermodynamically favorable reactions typically occur where labile electron donors (e.g., organic matter) come in contact with oxygenated water masses (e.g., the top of the sediment column). Such chemical gradients are common where sediments are well stratified, predominantly where bioturbation or abiotic mixing (e.g., wave activity) does not occur. At the boundaries between gradients, chemical species interact, providing niches for microbial metabolic activity to catalyze these reactions.

Sulfate Reduction

In marine sediments, sulfate reduction occurs in the anoxic zone, below the depth at which oxygen has been depleted and often below the depth at which oxidized metal phases such as Mn^{4+} and Fe^{3+} oxides are reduced. Sulfate reduction is a strictly anaerobic metabolism, although oxygen exposure can be tolerated by many sulfate-reducing microorganisms (Cypionka 2000). Sulfate reduction may be coupled to the oxidation of H_2 or organic compounds such as acetate, lactate, malate, succinate, fumarate, fructose, glucose, or fatty acids (Rabus et al. 2013). Some strains of sulfate reducers are complete oxidizers, meaning that the organic substrate is quantitatively oxidized to CO_2 . Many sulfate reducers, however, are incomplete oxidizers, meaning that oxidation to CO_2 is nonquantitative, with the balance of carbon released as short-chain organic acids (e.g., acetic acid).

The organic compounds in marine sediments are typically derived directly or indirectly from the remnants of primary productivity. Ancient organic material may also fuel sulfate reduction, and some strains of sulfate reducers can directly oxidize thermogenic organic compounds, such as ethane, propane, and butane (Kniemeyer et al. 2007). Microorganisms can also couple the anaerobic oxidation of methane (AOM) (Hoehler et al. 1994) and other short-chain alkanes (Kniemeyer et al. 2007) to sulfate reduction. The mechanisms by which this process occurs are not fully understood (Knittel & Boetius 2009, Milucka et al. 2012) but are typically thought to involve a syntrophic consortium between archaea and sulfate-reducing bacteria (Boetius et al. 2000, Orphan et al. 2001).

The biochemistry of sulfate reduction has been increasingly well understood in the past several years (Oliveira et al. 2008, Venceslau et al. 2014). The process as currently understood is shown schematically in **Figure 1**. Microbial sulfate reducers first must transport sulfate from the environment into the cell via sulfate transporter proteins. These transporters are often symporters that cotransport sulfate anions along with protons or sodium ions (Cypionka 1995).

Diagenesis: physical and chemical changes occurring in sediments after their deposition (e.g., during lithification and burial)

Electron donor: chemical species (e.g., organic carbon) that donates electrons during cellular respiration, resulting in the release of energy

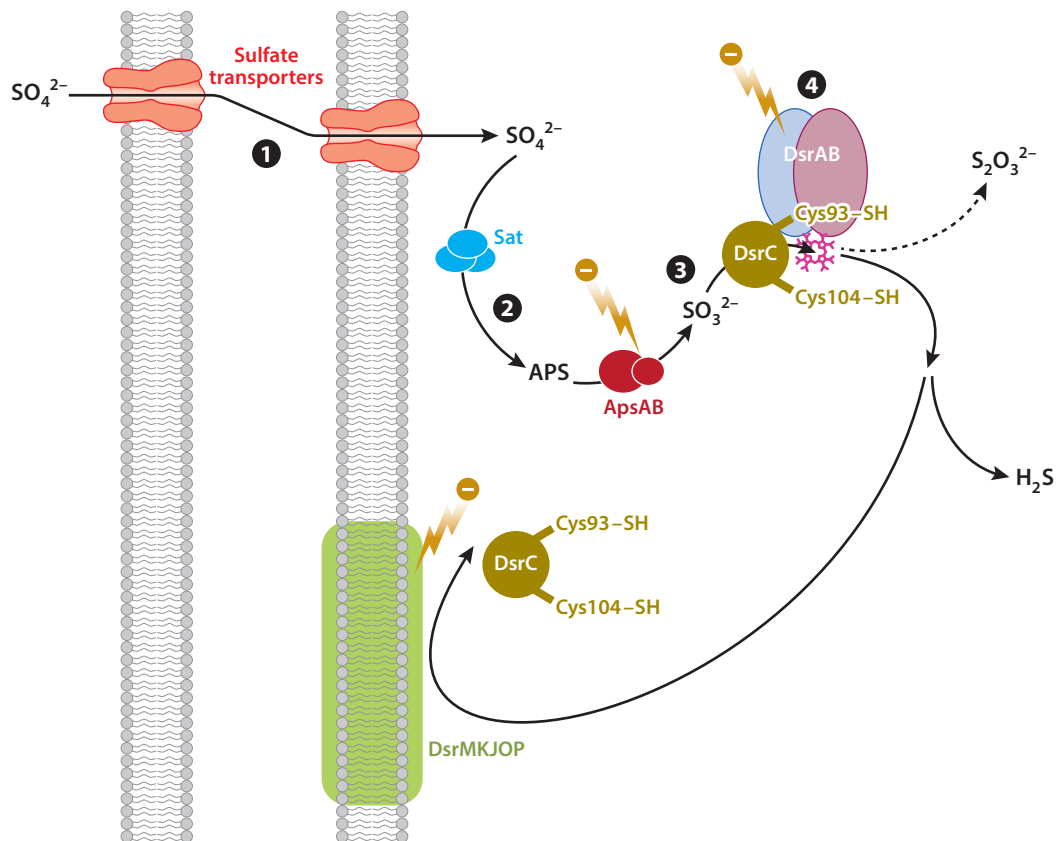


Figure 1

Schematic of the processes involved in dissimilatory sulfate reduction. (1) Sulfate is transported into the cytoplasm through the cell envelope. (2) ATP sulfurylase (Sat) activates sulfate to adenosine 5'-phosphosulfate (APS). (3) APS reductase (ApsAB) reduces APS to sulfite. (4) Sulfite interacts with the DsrABC complex [composed of the dissimilatory sulfite reductase (DsrAB) and a sulfur transfer protein (DsrC)]. This interaction is complex and *in vitro* can produce a range of direct products, including trithionate, thiosulfate, and sulfide. Partially reduced sulfur bound to DsrAB can yield thiosulfate. Generally, four electrons are transferred by DsrAB, and zero-valent sulfur is bound to DsrC, which undocks from DsrAB and carries S as an intermediate redox state to the DsrMKJOP complex (Venceslau et al. 2014). The structure of this intermediate state of DsrC bound to the partially reduced S from DsrAB is still under investigation. DsrC acts as an electron acceptor that interacts with the energy-conserving complex in the cell membrane (DsrMKJOP) (Venceslau et al. 2014), regenerating reduced DsrC that can redock with DsrAB, with concomitant release of sulfur as H_2S . Sites of electron donation are indicated by orange lightning bolts.

Genomes of sulfate reducers, such as *Desulfovibrio* spp. (Hauser et al. 2011), suggest that there are diverse sulfate transporters in these microbes, including both diffusion-controlled symporters and ATP-dependent transporters. Energetic considerations favor passive transport as the more likely mechanism during dissimilatory metabolism (Cypionka 1995). The cellular half-saturation constants for sulfate ($K_{S-\text{SO}_4}$) in sulfate-reducing bacteria have a wide range of values, from as low as 3 μM to more than 5 mM (see the review in Tarpgaard et al. 2011). These values may relate to the expression of sulfur isotope fractionation during sulfate reduction (Habicht et al. 2002; see below).

Inside the cytoplasm, sulfate reduction proceeds when sulfate is activated by the enzyme ATP sulfurylase (Sat) to adenosine 5'-phosphosulfate (APS). This is necessary due to the unfavorable thermodynamics of the reduction of sulfate to sulfite ($\Delta E_0' = -516 \text{ mV}$ for $\text{SO}_4^{2-}/\text{HSO}_3^-$), which

strongly favors sulfate. APS reduction to sulfite is more energetically favorable ($\Delta E_0' = -60$ mV for APS/AMP + HSO₃⁻), but the conversion to APS requires the cell to invest a molecule of ATP.

Subsequently, APS is reduced to sulfite by the enzyme APS reductase (ApsAB) (Michaels et al. 1970). Sulfite is a key intermediate in dissimilatory sulfate reduction. Sulfite is reduced by two enzymes, the dissimilatory sulfite reductase (DsrAB) and a sulfur transfer protein (DsrC), via a complex set of reactions involving all three subunits (DsrABC) (Venceslau et al. 2014). First, sulfite is bound to the active site of DsrAB and reduced via two sets of two-electron transfers—producing intermediates in the S²⁺ or S⁰ reduction state that nominally remain bound to the active site. After four electrons have been transferred, the partially reduced sulfur in the active site forms a persulfide bond with a cysteine residue on the DsrC subunit, which subsequently undocks from DsrAB and freely moves in the cytoplasm (Oliveira et al. 2008). These details and those of the next stage are not perfectly understood, but it has been postulated that DsrC expunges the bound sulfur as hydrogen sulfide, and oxidized DsrC then interacts with the DsrMKJOP complex at the cell membrane, where it acts as an electron acceptor (Oliveira et al. 2008, Venceslau et al. 2014). In this way, DsrC is directly coupled to the respiratory electron chain at the inner membrane, contributing to energy conservation.

This set of reactions explains many years of data on cell-free extracts and isolated *in vitro* DsrAB, in which sulfite was converted to a mixture of trithionate and thiosulfate (Kobayashi et al. 1972, Peck 1962). These data inspired the proposed trithionate pathway of sulfate reduction, in which both trithionate and thiosulfate are intermediates between sulfite and hydrogen sulfide (Drake & Akagi 1977). However, the presence of thiosulfate and trithionate in the *in vitro* experiments can be explained by excess sulfite reacting with partially reduced sulfur (in the S²⁺ or S⁰ state) at the active site (Chambers & Trudinger 1975). *In vivo*, these reactions are not likely to be quantitatively important at high sulfate reduction rates. However, sulfate-reducing bacteria may produce thiosulfate and trithionate, particularly under oxidizing conditions (Sass et al. 1992), where the supply rate of sulfite to the active site may be higher than usual relative to the supply rate of electrons (Bradley et al. 2011).

The fractionation of sulfur isotopes at each of these steps has not been well constrained. Rees (1973) proposed that both APS reduction and sulfite reduction are associated with discrimination against ³⁴S by a factor of 25‰ whereas sulfate transport has an inverse fractionation of 3‰ (meaning the product is heavy relative to the reactant). This proposal was consistent with a maximum observed fractionation of 47‰, which is in line with observed fractionations in pure cultures (Canfield & Teske 1996). The proposed trithionate pathway, and the observation of large fractionations in sediments, suggested that the Rees model was not sufficient to describe observed isotope fractionations (although see the discussion of disproportionation, below). Subsequent to the study by Canfield & Teske (1996), one pure culture has been observed to produce fractionations >65‰ (Sim et al. 2011a) in batch cultures, as have mixed cultures of modern lacustrine waters (Canfield et al. 2010), and values above 55‰ have been observed with well-studied strains in chemostat cultures (Leavitt et al. 2013a). Isolated DsrAB produces a fractionation *in vitro* of 15.3‰ (Leavitt et al. 2013b), which is substantially smaller than the fractionation for sulfite reduction predicted by isotope models (Brunner & Bernasconi 2005, Harrison & Thode 1958, Rees 1973). Whatever the details of the isotope fractionations produced by the enzymatic machinery, two clear parameters have been shown to significantly affect the expressed sulfur isotope fractionation during sulfate reduction. The first is the sulfate concentration—increased sulfate concentrations yield increased fractionations up to a strain-specific threshold (Habicht et al. 2002). The second is the cell-specific sulfate reduction rate (csSRR), with faster rates yielding smaller fractionations (**Figure 2**) (Chambers et al. 1975; Harrison & Thode 1958; Kaplan & Rittenberg 1964; Leavitt et al. 2013a; Sim et al. 2011a,b, 2012). Recent work has suggested that slower rates allow

Cell-specific sulfate reduction rate

(csSRR): impacts the expression of isotopic fractionation during microbial sulfate reduction

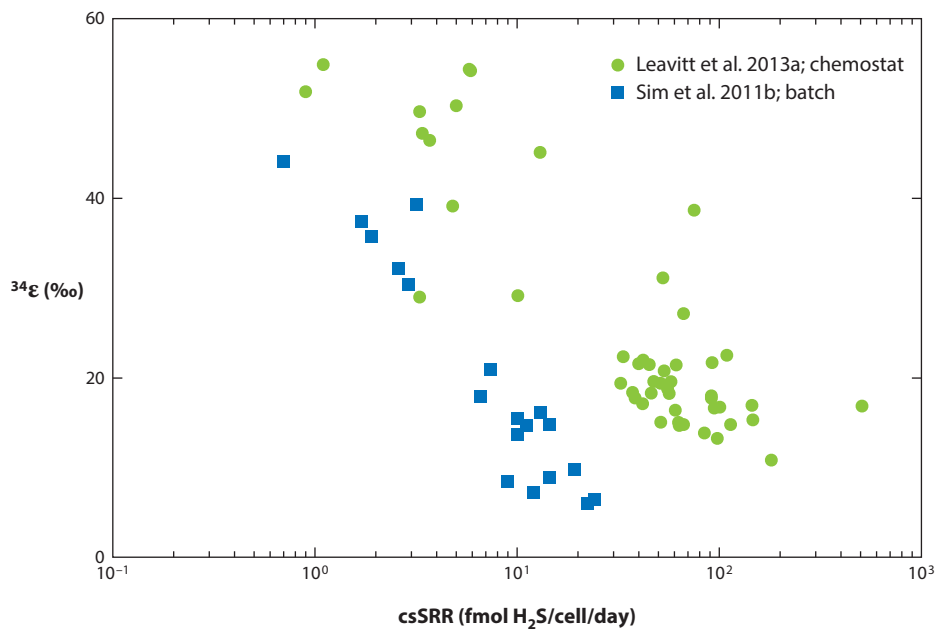


Figure 2

Relationship between isotope fractionation during sulfate reduction and cell-specific sulfate reduction rate (csSRR) in *Desulfovibrio vulgaris* str. Hildenborough. There is a trend toward decreased fractionation ($^{34}\epsilon$) during sulfate reduction at increased csSRR. Data derived from Leavitt et al. (2013a) and Sim et al. (2011b).

the sulfur isotope fractionation to approach thermodynamic equilibrium, whereas faster rates express a more purely kinetic sulfur isotope fractionation (Wing & Halevy 2014).

Sulfide Oxidation

Sulfate reduction converts sulfate to sulfide (**Figure 3a**, blue). Sulfide oxidation reverses this process, via the conversion of hydrogen sulfide or sulfide minerals to more oxidized sulfur species (**Figure 3a**, green). Like sulfate reduction, sulfide oxidation can be coupled to energy conservation. In addition, the electrons supplied by reduced sulfur species can be used for autotrophic carbon fixation. Several enzymatic systems exist for the oxidation of hydrogen sulfide to sulfate, either directly or through intermediary pools of elemental sulfur. The *sox* gene cluster encodes the most well studied pathway. The complete set of genes, extensively characterized in *Paracoccus pantropus* (Friedrich et al. 2001, 2005), transforms hydrogen sulfide to sulfate, using oxygen as an electron acceptor. In many organisms, a truncated version of this aerobic pathway transforms hydrogen sulfide to soluble elemental sulfur (Friedrich et al. 2001, 2005). Transformation of hydrogen sulfide to sulfur is also accomplished by anaerobic phototrophs such as *Rhodobacter* spp., using a partial *sox* pathway that does not include the *soxCD* genes. Phototrophs such as *Chlorobium* and *Allochromatium* spp. store sulfur intracellularly as elemental sulfur globules and are able to complete the transformation to sulfate via enzymes encoded by the *dsr* gene cluster (Dahl et al. 2005). Sulfide-oxidizing archaea found in the order Sulfolobales lack the *sox* cluster and contain a distinct system for sulfide oxidation (Friedrich et al. 2001, 2005; Ghosh & Dam 2009).

Isotopic fractionation during biological sulfide oxidation is generally considered to be negligible (Canfield 2001a). Abiotic oxidation of sulfide to sulfur, thiosulfate, sulfite, or sulfate can produce

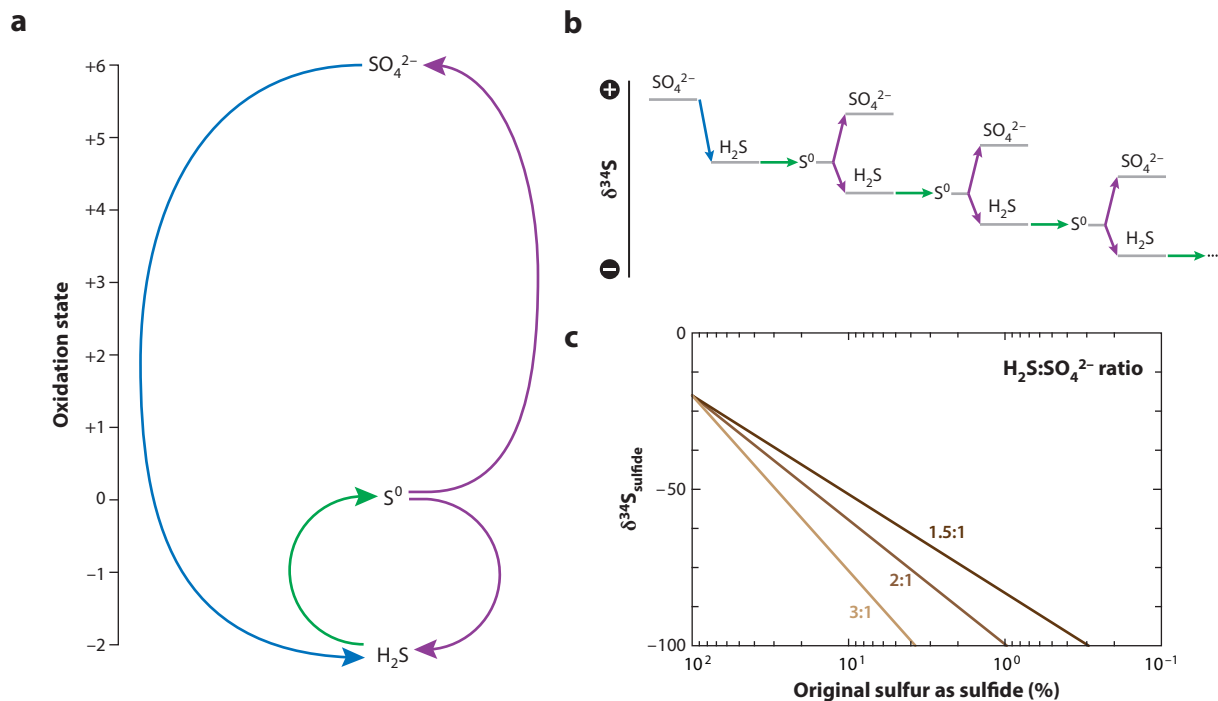


Figure 3

(a) Major microbial sulfur cycling metabolisms and their redox transformations: Sulfate reduction (blue) transforms sulfate (+6) to sulfide (−2); sulfide oxidation (green) transforms sulfide to a more oxidized state between S^0 (shown) and S^{+6} ; and disproportionation of elemental sulfur (purple) (or other intermediate-valence sulfur species) transforms S^0 to H_2S and SO_4^{2-} . (b) Isotopic impact of disproportionation (after Canfield & Thamdrup 1994). Sulfate reduction results in sulfide that is depleted in ^{34}S . Subsequent cycles of oxidation (minimal isotopic fractionation) and disproportionation (yielding ^{34}S -enriched sulfide and ^{34}S -depleted sulfide) can produce H_2S that is increasingly depleted in ^{34}S . (c) The $\delta^{34}\text{S}$ of sulfide that can be produced by this process is related to the ratio of H_2S to SO_4^{2-} generated in each cycle, the fractionation at each step, and the amount of initial sulfate converted to sulfide in a closed system. The schematic in panel b shows a process in which sulfate reduction results in initial sulfide at -15‰ , and subsequent cycles of oxidation and disproportionation each yield an additional 7‰ depletion in ^{34}S . The relationship between H_2S yield and $\delta^{34}\text{S}$ is shown for three ratios of H_2S to SO_4^{2-} .

fractionations as large as 5‰ (Fry et al. 1988), but demonstrated biological fractionations during both aerobic sulfur oxidation and phototrophic sulfur oxidation are on the order of $1\text{--}2\text{‰}$ (Fry et al. 1984, 1985; Zerkle et al. 2009). One exception is an early study by Kaplan & Rittenberg (1964) in which the oxidation of sulfide to sulfate by *Thiobacillus concretivorus* (now *Acidithiobacillus thiooxidans*) was associated with an isotope fractionation of up to 18‰ , but simultaneously produced elemental sulfur depleted by only 2.5‰ . Although this result has not been revisited, fractionations associated with sulfide oxidation are generally assumed to be small. Nonetheless, oxidative processes may play important roles in modulating $\delta^{34}\text{S}$ signals in depositional environments (e.g., shallow marine settings) characterized by frequent, repeated oxidative reworking (Aller 2014; see below).

Sulfur Disproportionation

Because oxidation of sulfide can yield sulfur compounds of intermediate valence, organisms have evolved to take advantage of these compounds by simultaneously using them as electron donors and

acceptors—that is, performing sulfur disproportionation (**Figure 3a**, purple). Sulfur compounds of intermediate valence appear in the environment following sulfide oxidation, so the presence of disproportionation in the rock record is thought to postdate the evolution of an oxidative sulfur cycle (Canfield & Teske 1996, Canfield & Thamdrup 1994, Johnston et al. 2005b). The ability to perform sulfur disproportionation coupled to energy metabolism is common among strains of sulfate reducers and can be found in *Desulfovibrio*, *Desulfobacter*, and *Desulfocapsa* spp., among others. Disproportionation of sulfite and thiosulfate is thermodynamically favorable under standard physiological conditions (1 M concentrations of all reactants and products at pH 7), whereas disproportionation of S^0 is not (Finster 2008). In order for S^0 disproportionation to be thermodynamically favorable, the sulfide product must remain at low concentrations (<1 mM; Finster 2008), often requiring it to be scavenged by iron or manganese (Böttcher & Thamdrup 2001). The net stoichiometry of S^0 disproportionation is



but the net stoichiometry changes when sulfide is scavenged by iron (Canfield & Thamdrup 1996):



The biochemistry of the disproportionation reactions is less well understood than that of sulfate reduction or sulfide oxidation. However, there is evidence that sulfate reduction enzymes play a role in disproportionation of thiosulfate, and possibly of S^0 (Finster 2008). Disproportionation of S^0 has been a focus of isotope geochemists because S^0 is abundant in sediments (Troelsen & Jørgensen 1982) and is actively disproportionated (Canfield & Thamdrup 1996). Furthermore, recent work on AOM also suggests a role for the disproportionation of disulfide (S_2^{2-}) (Milucka et al. 2012).

Disproportionation has been proposed as a mechanism for producing large ^{34}S depletions in sedimentary sulfides (Canfield & Teske 1996, Canfield & Thamdrup 1994). The mechanism for this is schematically illustrated in **Figure 3b**. Initial sulfate reduction produces sulfide that is depleted in ^{34}S relative to sulfate by an amount consistent with sulfate reduction (i.e., up to 47‰ and possibly larger; see Leavitt et al. 2013a; Sim et al. 2011a,b). This sulfide may then be oxidized to S^0 with minimal isotope fractionation. Subsequent disproportionation of the S^0 produces sulfide that is further depleted in ^{34}S and sulfate that is enriched in ^{34}S relative to S^0 . Sulfide produced via this process is depleted by approximately 4–9‰ relative to S^0 (Böttcher et al. 2001, Canfield & Thamdrup 1996, Habicht et al. 1998), although the mechanism of oxidation is important, and the depletion is much smaller if the process occurs via manganese oxides rather than iron oxides (Böttcher & Thamdrup 2001). Through repeated cycles of sulfide oxidation to S^0 (with negligible fractionation) and S^0 disproportionation, increasingly ^{34}S -depleted sulfide can be generated (**Figure 3b**) (Canfield & Teske 1996, Canfield & Thamdrup 1994). Because each cycle generates sulfate (which is assumed to be freely exchangeable with the overlying water column) as well as sulfide, the fraction of initial sulfur remaining decreases with each iterative cycle. In a closed system, the amount of sulfide mineral that can be generated at a given $\delta^{34}S$ is a function of the ratio of sulfide to sulfate produced during the disproportionation process: A higher ratio allows a greater amount of ^{34}S -depleted sulfide (**Figure 3c**). The 3:1 net stoichiometry of disproportionation could in principle produce large (>60‰) depletions while yielding more than 10% of the initial sulfur in the system. The 2:1 sulfide to sulfate ratio required by iron scavenging can produce similarly large fractionations, but only with a decreased yield of sulfide minerals. In practice, even lower ratios—closer to 1.5:1—are observed in experiments, with the missing sulfide presumably incorporated into biomass (Canfield & Thamdrup 1996), resulting in commensurately smaller yields of sulfide to produce large isotopic depletions.

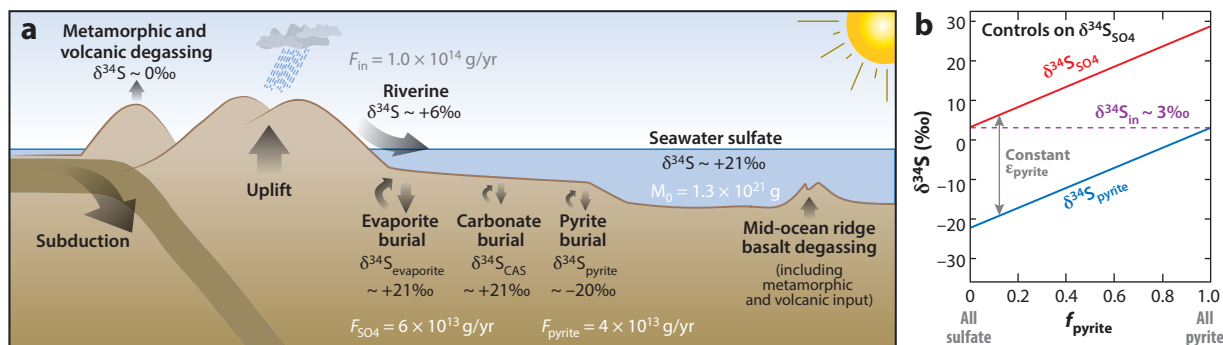


Figure 4

(a) Schematic of the geological sulfur cycle, characterized by a large seawater sulfate reservoir ($M_0 = 1.3 \times 10^{21}$ g; $\delta^{34}\text{S}_{\text{SO}_4} = 21\text{‰}$). Input fluxes (F) are derived from a mixture of weathering, volcanic, and hydrothermal activity, with a combined isotopic composition of $\sim 3\text{‰}$. There are two major sinks: sulfate and pyrite. Sulfate is buried in the form of marine evaporites, which can weather quickly, as well as carbonate-associated sulfate (CAS); the isotopic composition of sulfate in both of these sinks is similar to that of seawater sulfate. The pyrite sink represents sulfide captured following microbial sulfate reduction, which is associated with a typical isotopic fractionation of $\sim 40\text{‰}$ (i.e., $\delta^{34}\text{S}_{\text{pyrite}} \approx \delta^{34}\text{S}_{\text{SO}_4} - 40\text{‰}$). (b) Schematic showing the steady-state dependence of marine $\delta^{34}\text{S}_{\text{SO}_4}$ on the relative burial flux of sulfides (f_{pyrite}), the isotopic fractionation between coeval sulfate and sulfides (ϵ_{pyrite}), and the isotopic composition of sulfate entering the oceans ($\delta^{34}\text{S}_{\text{in}}$). Flux and isotopic parameters from Kah et al. (2004), Canfield (2004).

The discovery that sulfate reduction alone, when occurring at slow rates, can produce large fractionations (up to 66‰) has complicated the standard interpretation that isotopic offsets between sulfate and sulfide above 47‰ require disproportionation (e.g., Canfield & Teske 1996, Fike et al. 2006, Parnell et al. 2010). These data suggest that fractionations up to 66‰ could result from either sulfate reduction alone or a combination of sulfate reduction and disproportionation. Additional information (e.g., microbial community composition, depositional context, ambient geochemistry, and studies that quantitatively account for all reactants and products) is needed to tease apart these different cases.

GEOLOGICAL SULFUR CYCLING

The modern geological sulfur cycle (**Figure 4a**) centers on sulfur's largest biologically available reservoir, dissolved marine sulfate, and in many ways the sulfur cycle mirrors the carbon biogeochemical cycle (see sidebar, Comparing the Carbon and Sulfur Cycles). Marine sulfate concentrations are 28 mM (corresponding to 1.3×10^{21} g of S, the fourth most abundant solute in seawater). Sulfate concentrations are conservative in oxygenated waters, with concentrations increasing and decreasing only due to evaporation and freshening from meteoric fluids. Sulfate represents the largest oxidant pool in the oceans—equivalent to more than 10 times the oxidizing capacity of present atmospheric oxygen levels (Hayes & Waldbauer 2006). With an estimated flux of 1.0×10^{14} g/yr into (and out of) the ocean, the oceanic sulfate reservoir has a long response time (~ 13 Myr) (Kah et al. 2004). However, sulfate concentrations in the ocean are thought to have changed substantially over Earth history, driven by imbalances in the fluxes into and out of the ocean (Brennan et al. 2004, Canfield 2004, Halevy et al. 2012, Holland 1973, Horita et al. 2002, Lowenstein et al. 2003, Wortmann & Chernyavsky 2007, Wortmann & Paytan 2012). Marine sulfate is replenished by the input of sulfur from riverine weathering, hydrothermal and volcanic sources, dust, and biogenic gases, as well as the biotic or abiotic oxidation of hydrogen sulfide to sulfate. Sulfate is removed from the ocean predominantly as sulfate evaporite minerals (gypsum

Evaporite: chemical precipitate formed from the evaporation of seawater in a partially restricted basin with limited connection to the open ocean

COMPARING THE CARBON AND SULFUR CYCLES

In many ways, the carbon and sulfur cycles are quite similar. They share a single large oxidized oceanic reservoir (dissolved inorganic carbon for carbon, sulfate for sulfur) and an input flux from weathering, volcanic activity, and hydrothermal activity, and both have two major ocean sinks: an oxidized flux that mirrors the ocean reservoir (calcium carbonate and sulfate minerals, respectively) and a reduced flux isotopically fractionated by microbial activity (organic carbon and pyrite, respectively). However, there are significant differences. First, the carbon cycle has a fast response time (driven by a relatively smaller dissolved inorganic carbon reservoir and large flux), whereas the sulfur cycle has a slower response time (driven by smaller flux into a larger sulfate reservoir). More importantly, the flux of reduced carbon (organic matter) is sourced primarily from the water column, whereas the flux of reduced sulfur (pyrite) is formed primarily within the sediments. These differences necessitate care when trying to link isotopic signatures of carbon and sulfur cycling preserved in sedimentary records.

or anhydrite), as well as through carbonate-associated sulfate (CAS), sulfate bound into the carbonate mineral lattice (Burdett et al. 1989), or barite, with minor fluxes out of the ocean through salt deposition and as biogenic gases. In addition, sulfate can be removed via conversion to hydrogen sulfide during microbial sulfate reduction (see above). The vast majority (>90%) of sulfide formed from sulfate reduction is typically reoxidized back to sulfate (Jørgensen 1982). However, a fraction of the hydrogen sulfide can be scavenged by reactive iron to produce metastable iron sulfide (FeS) minerals and eventually pyrite (FeS₂) (Berner 1984, Rickard 1995, Rickard & Luther 1997). There is thought to be minimal isotopic fractionation associated with the conversion from hydrogen sulfide to pyrite. The resulting burial of sedimentary pyrite and that of sulfate evaporites are the dominant pathways by which sulfur leaves the ocean (**Figure 4a**). It is through the microbial processing of sulfate and the generation of biogenic pyrite that the microbial sulfur cycle imprints itself on the geological sulfur cycle. The availability of reactive iron provides additional modulation on the ability to preserve hydrogen sulfide as pyrite, illustrating the tight linkages between the iron and sulfur geochemical cycles.

The two main factors driving the long-term secular variation in the isotopic composition of sulfur species over geological time are variations in (a) the net flux of sulfate reduced to sulfide and preserved as pyrite in marine sediments and (b) the mean isotopic fractionation associated with the metabolic networks that generate this net flux of pyrite from the starting reactant, marine sulfate, to the final product, hydrogen sulfide and, ultimately, reduced iron sulfide minerals. Additional variation can be driven by both short-term (Halevy et al. 2012, Wortmann & Chernyavsky 2007, Wortmann & Paytan 2012) and long-term (Canfield 2004, Fike & Grotzinger 2008) changes to the flux and isotopic composition of sulfate delivered to the ocean. It is changes in these three parameters—relative burial flux of sulfides (f_{pyrite}), isotopic fractionation between coeval sulfate and sulfides (ϵ_{pyrite}), and isotopic composition of riverine input ($\delta^{34}\text{S}_{\text{in}}$)—that drive secular change in sulfur isotopic records. These parameters are linked together in the standard steady-state description of isotopic mass balance in the sulfur cycle:

$$\delta^{34}\text{S}_{\text{in}} = (1 - f_{\text{pyrite}}) \times \delta^{34}\text{S}_{\text{SO}_4} + f_{\text{pyrite}} \times \delta^{34}\text{S}_{\text{pyrite}}$$

This can be further simplified by substitution of $\epsilon_{\text{pyrite}} = \delta^{34}\text{S}_{\text{SO}_4} - \delta^{34}\text{S}_{\text{pyrite}}$ to obtain the following:

$$\delta^{34}\text{S}_{\text{SO}_4} = \delta^{34}\text{S}_{\text{in}} + f_{\text{pyrite}} \times \epsilon_{\text{pyrite}}$$

This form illustrates the control these three parameters have on marine $\delta^{34}\text{S}_{\text{SO}_4}$ values, seen graphically in **Figure 4b**.

Carbonate-associated sulfate (CAS):

sulfate substituting within the carbonate mineral matrix, often at levels between 100 and 10,000 ppm

f_{pyrite} : the fraction of sulfur leaving the ocean that is buried as pyrite (rather than as sulfate)

ϵ_{pyrite} : the apparent ^{34}S isotopic fractionation between co-occurring sulfate and pyrite

$\delta^{34}\text{S}_{\text{in}}$: the average $\delta^{34}\text{S}$ composition of sulfur entering the ocean

Table 1 Qualitative comparison of sulfate proxies for seawater $\delta^{34}\text{S}_{\text{SO}_4}$ ^a

Proxy	Accuracy	Robustness	Temporal continuity	Spatially continuity	Ease of extraction and analysis
Sulfate evaporites ^b	●●●	●●●●	●	●	●●●●●
Barite	●●●●●	●●●●●	●●● ^c	●●●●●	●
Carbonate-associated sulfate	●●●	●●●	●●●●●	●●●● ^d	●●●

^aQualitative evaluation from high (●●●●●) to low (●). See text for details.

^bSulfate evaporites include gypsum and anhydrite.

^cBarite record relies on deep-sea sediment cores and to date extends back only through the Cretaceous.

^dPrior to the onset of calcareous plankton, carbonate precipitation was limited to the shallow sea and continental slope.

Deep-time records of sulfur cycling are dominated by records of marine sulfate and/or pyrite (Canfield 2001a, Strauss 1997). Sulfate records come primarily from sulfate evaporites [gypsum or anhydrite (Claypool et al. 1980, Holser 1977)], marine barites (Paytan et al. 1998, 2004), or CAS (Burdett et al. 1989, Kampschulte & Strauss 2004). Time-series $\delta^{34}\text{S}$ records through specific stratigraphic intervals provide the data used for these reconstructions of global sulfur biogeochemical cycling (see below).

MINERAL RECORDS OF SULFIDE AND SULFATE $\delta^{34}\text{S}$

Reconstructions of the ancient sulfur cycle are based on relating the $\delta^{34}\text{S}$ composition of a measured sulfate or sulfide phase to the marine $\delta^{34}\text{S}_{\text{SO}_4}$ composition. Thus, when interpreting stable sulfur isotopic data in the geological record, it is essential to be cognizant of the depositional environment in which the sample formed, its connection to the open ocean, and its subsequent diagenetic history. Three primary proxies exist for reconstructing the $\delta^{34}\text{S}_{\text{SO}_4}$ of ancient seawater sulfate: sulfate evaporite minerals such as gypsum and anhydrite; barite; and CAS. Each proxy has different characteristics in terms of its environment of formation, susceptibility to alteration during and after deposition, and ease of analysis (**Table 1**).

Evaporite-based records provided our earliest understanding of the long-term evolution of the sulfur cycle and identified many of the first-order trends in $\delta^{34}\text{S}_{\text{SO}_4}$ over Earth history (Claypool et al. 1980, Holser 1977). However, evaporites are deposited in partially restricted basins, which have limited connection to the open ocean, and in which evaporation rates exceed the influx of marine water. Such evaporite deposits represent both spatially and temporally discontinuous samplings of the open ocean. Furthermore, by their nature evaporites represent fluids that have chemically evolved from open marine waters, and the sulfate they contain may not reflect open marine conditions. During the process of evaporite formation, the $\delta^{34}\text{S}_{\text{SO}_4}$ can shift to lower values due to the fractionation ($\sim 1.6\text{‰}$) associated with gypsum deposition (Raab & Spiro 1991), or to higher values if there is ongoing pyrite formation during basin restriction (Fike & Grotzinger 2010). Mass balance constraints, however, generally limit the magnitude of these shifts to less than a few permil (Fike & Grotzinger 2010, Raab & Spiro 1991)—that is, small compared with the magnitude of change ($\sim 40\text{‰}$) in $\delta^{34}\text{S}_{\text{SO}_4}$ over Earth history (Canfield 2001a).

Barite (BaSO_4) can form in many environments, including in the open marine water column, within sediments, and in hydrothermal settings (Paytan et al. 2002). Marine barites can be identified by crystal morphology, size, and chemistry and can be analyzed for their $\delta^{34}\text{S}$ composition (Paytan et al. 2002). Barite-derived time-series $\delta^{34}\text{S}_{\text{SO}_4}$ records are among the most well resolved, but they require painstaking screening, and to date, barite records from select sediment cores and locations extend back only through the Cretaceous (Paytan et al. 1998, 2004).

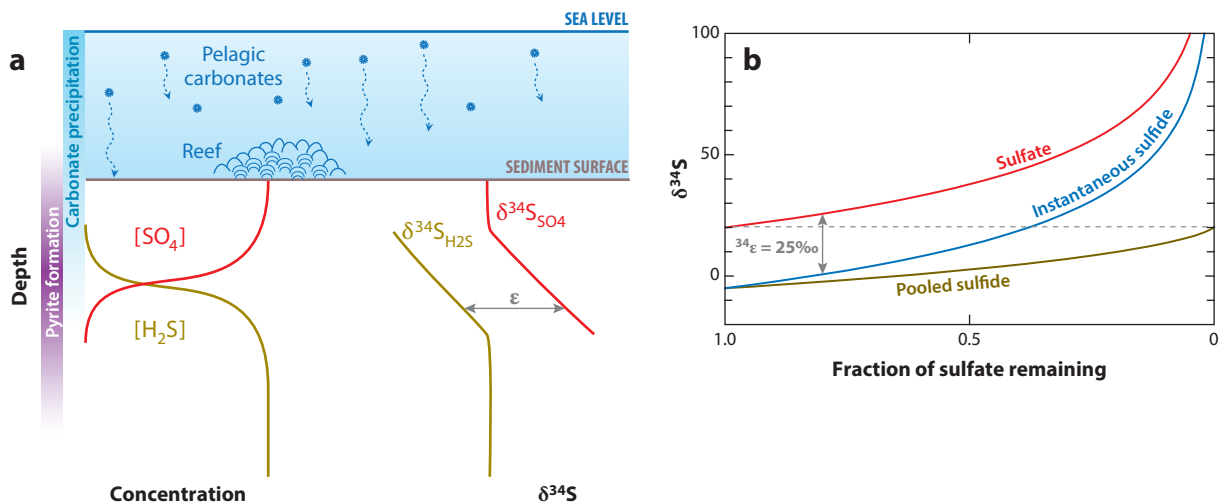


Figure 5

(a) Schematic showing the incorporation of carbonate-associated sulfate in marine carbonates. Carbonate precipitation (left, light blue) can occur in the water column, at the seafloor, or in the sediment, especially in the presence of sulfate reduction. Microbial sulfate reduction (here shown with a constant ϵ) in the sediments results in the production of H_2S , the abundance and isotopic composition of which depend on depth. The sulfide $\delta^{34}S$ signature can be encoded in pyrite (left, purple) following reaction with iron. (b) Schematic showing the isotopic evolution of sulfate and sulfide during closed-system sulfate reduction (at constant ϵ).

Most of the data used to reconstruct ancient $\delta^{34}S_{SO_4}$ derive from measurements of CAS (Burdett et al. 1989). CAS is incorporated during both abiotic and biological carbonate precipitation (Staudt et al. 1994, Staudt & Schoonen 1995, Takano 1995) and thus occurs predominantly within the water column and near the sediment/water interface (**Figure 5a**). These carbonates likely reflect water column chemistry, and thus $\delta^{34}S_{CAS}$ approximates marine $\delta^{34}S_{SO_4}$ (Burdett et al. 1989). Additional carbonate cementation can also occur beneath the sediment/water interface, particularly associated with anaerobic respiration (e.g., sulfate reduction) (Visscher et al. 2000). This carbonate precipitation can impact $\delta^{34}S_{CAS}$ if substantial carbonate precipitation occurs where the isotopic composition of the local pool of sulfate has been impacted by microbial metabolic activity. For example, above the sulfide-oxygen chemocline, oxidation of ^{34}S -depleted hydrogen sulfide diffusing from below can decrease $\delta^{34}S_{SO_4}$; below the chemocline, ongoing microbial sulfate reduction can increase $\delta^{34}S_{SO_4}$ in the residual sulfate pool. If there is active carbonate precipitation in these zones, the resulting $\delta^{34}S_{CAS}$ record can be altered to higher (or lower) values depending on whether precipitation occurs in the zone of net sulfate reduction (or sulfide oxidation). More work needs to be done to understand the potential syndepositional and diagenetic processes that may give rise to $\delta^{34}S_{CAS}$ variability.

The deep-time sulfide $\delta^{34}S$ record is derived predominantly from pyrite. Pyrite forms when reactive iron reacts with hydrogen sulfide (Rickard 1995, Rickard & Luther 1997) sourced primarily from microbial sulfate reduction. During the course of sulfate reduction, the residual sulfate pool shrinks and $\delta^{34}S_{SO_4}$ increases, undergoing Rayleigh-type distillation (**Figure 5b**). Independent of any change in biological fractionation, this distillation results in a parallel increase in $\delta^{34}S_{H_2S}$ that can then be preserved in $\delta^{34}S_{pyrite}$. The magnitude of this enrichment depends on the fraction of sulfate that is consumed, the connectivity between the pore water sulfate pool and the overlying water column, and the fractionation associated with the redox transformation itself. These factors depend on sulfate concentration, organic carbon loading, sedimentation rate, and sediment porosity

IMPACT OF DEPOSITIONAL ENVIRONMENT

Frequently, $\delta^{34}\text{S}$ data are used to make direct reconstructions of ocean chemistry. However, it is increasingly clear that the sedimentary environment of deposition can have dramatic impacts on the abundance and isotopic composition of both sulfate and sulfide. $\delta^{34}\text{S}$ data, from both pyrites and CAS, need to be placed in a detailed sedimentological context before stratigraphic variations in these records can be understood. Characteristics of or changes in the local depositional environment can easily give rise to $\delta^{34}\text{S}$ signals that might otherwise be interpreted to reflect ocean chemistry.

or permeability (Aller 2014, Canfield 1991). Limited pore water exchange drives bulk $\delta^{34}\text{S}_{\text{H}_2\text{S}}$ to values approaching $\delta^{34}\text{S}_{\text{SO}_4}$, independent of biological fractionation. The degree to which this signal is transmitted to the $\delta^{34}\text{S}_{\text{pyrite}}$ record depends strongly on availability of reactive iron and the efficiency with which H_2S is converted to pyrite. The impact of closed-system distillation can be teased apart with high-resolution spatial analysis using secondary ion mass spectrometry (SIMS) to identify $\delta^{34}\text{S}$ gradients within individual pyrite crystals (Fischer et al. 2014). Understanding where a pyrite forms within a sedimentary column and how its environment was connected to the overlying water column is a necessary step before interpreting $\delta^{34}\text{S}_{\text{pyrite}}$ data to reconstruct sulfur cycling.

IMPACT OF DEPOSITIONAL ENVIRONMENT ON $\delta^{34}\text{S}$ RECORDS

Characteristics of the depositional environment can have an important role in modifying sulfur isotope signatures that are ultimately incorporated in marine sediments (e.g., Aller 2014; Aller et al. 2008, 2010; Canfield 1991; Canfield & Farquhar 2009; Ries et al. 2009). The impact of depositional environment on $\delta^{34}\text{S}$ signatures can manifest itself through multiple avenues, including (a) intrinsic characteristics of sediment (e.g., organic carbon loading, sedimentation rate, and sediment grain size and shape); (b) characteristics of the physical depositional environment (e.g., presence of tidal or storm-induced sediment remobilization); and (c) characteristics of macro- and microecology (e.g., bioturbation or presence of microbial mats) (see sidebar, Impact of Depositional Environment). These factors can change within a sedimentary basin and between different basins and, particularly in the case of the latter, are likely to have changed dramatically over Earth history.

Both sedimentary remobilization and bioturbation can impact $\delta^{34}\text{S}$ records by partial or complete oxidation of the reduced sulfur pools. Depositional environment and sediment remobilization can have considerable impacts on both the concentration and isotopic composition of both pore water and sedimentary sulfate and sulfide phases (Aller et al. 2008, 2010). For example, storm reworking of sediments or bioturbation can allow exchange of pools of sulfur and iron between reduced deeper layers and oxidized surface layers. This mixes isotopic signals that were previously stratified, and disturbs the idealized layering of geochemical processes (**Figure 6**). During this reworking (**Figure 6a**), the juxtaposition of newly deposited oxic sediments and those containing sulfide can result in H_2S oxidation, increasing residual $\delta^{34}\text{S}_{\text{H}_2\text{S}}$ (Fry et al. 1988). Subsequently, as oxygen is consumed (**Figure 6a**), the remobilized sediments transition into a phase of iron reduction, generating mobile Fe^{2+} that can react with this ^{34}S -enriched H_2S to form pyrite with elevated $\delta^{34}\text{S}_{\text{pyrite}}$ (Aller et al. 2008, Gao et al. 2013). This can potentially result in geochemical records that preserve small or negative isotopic offsets between sulfate and sulfide—differences that can be substantially less than the isotopic fractionation associated with microbial sulfur cycling in these sediments. This disconnect between microbial fractionations and isotopic offsets preserved in the

Sedimentary reworking: physical (e.g., through storm or tide activity) or biological mixing of sediments, often resulting in partial or complete oxidation of remobilized material

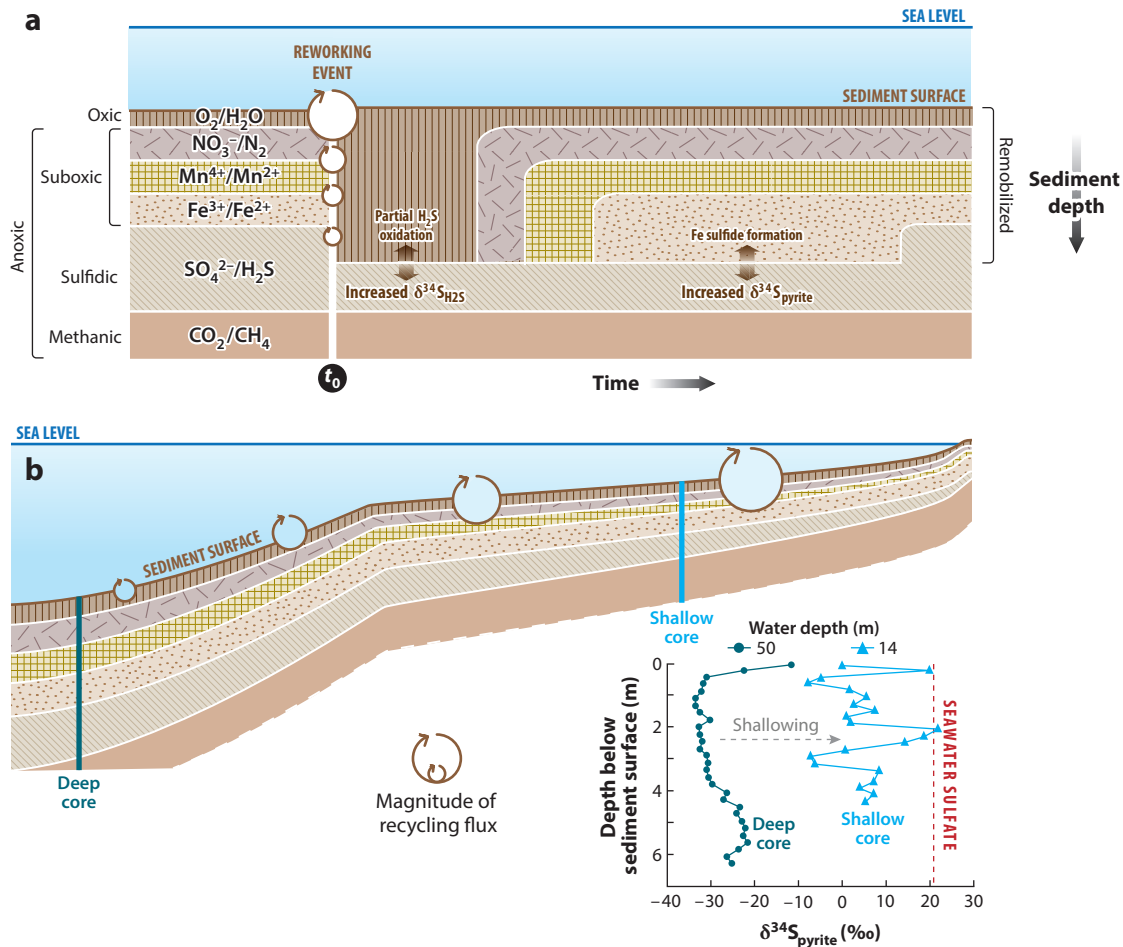


Figure 6

(a) Schematic showing the redox zonation by electron acceptor in a typical sediment profile. Following sedimentary reworking (t_0), remobilized sediment is variably oxidized and redeposited. Over time, redox zones return to normal as electron acceptors are preferentially consumed. The juxtaposition of oxic sediments and sulfidic sediments allows for the partial oxidation of H_2S and associated isotopic enrichment in $\delta^{34}S_{H_2S}$ (Fry et al. 1988). Subsequently, the transition to iron reduction in mobilized sediments provides a new source of Fe^{2+} that can react with this sulfide to form pyrite with elevated $\delta^{34}S_{pyrite}$. After Aller (2014). (b) Cross section of typical shallow slope sediments, showing that the magnitude of reworking decreases with depth. The inset shows a schematic of $\delta^{34}S_{pyrite}$ data from two cores taken at shallow (light blue) and deeper (dark blue) depths, highlighting the impact that reworking can have on both the mean values and stratigraphic variability of the $\delta^{34}S_{pyrite}$ signature. Isotope data are from Gao et al. (2013).

sediments could mislead investigators as to the nature of the processes that occurred in these environments.

PRESERVATION OF RECORDS

After deposition, both sulfate and pyrite $\delta^{34}S$ records have the potential to be altered by diagenetic processes. Records of $\delta^{34}S_{CAS}$ can be compromised during diagenesis by interaction with fluids (e.g., meteoric fluids or basinal brines) with a $\delta^{34}S_{SO_4}$ composition different from that of the

seawater in which they were deposited. Carbonate recrystallization under these conditions has the potential to alter the $\delta^{34}\text{S}_{\text{CAS}}$ record that is preserved. This alteration could be problematic as CAS is traditionally a bulk-rock measurement, and $\delta^{34}\text{S}_{\text{CAS}}$ reflects a phase-weighted average of components that may or may not be representative of syndepositional seawater sulfate. Microscale analysis of CAS capable of investigating these components individually would provide a means to assess such alteration. For example, owing to differential porosity, permeability, and crystal size, diagenetic processes are unlikely to affect all components (e.g., fossil fragments, lime mud, and various stages of marine cement) of a sample equally. The impact of syndepositional and diagenetic alteration on $\delta^{34}\text{S}_{\text{CAS}}$ can be assessed with coupled petrographic and geochemical analysis. Phase-specific differences in $\delta^{34}\text{S}_{\text{CAS}}$, particularly coupled with variations in CAS abundance, could indicate alteration of one or more phases. These observations can be tested with high-resolution analytical techniques (Fike & Jones 2012; Paris et al. 2013, 2014a,b) that have the potential to identify the origin of spatial variability in $\delta^{34}\text{S}_{\text{CAS}}$ records and to be combined with traditional indicators of carbonate diagenesis (Banner & Hanson 1990, Brand & Veizer 1980). The result would create a high-fidelity record of the evolution of the global sulfur cycle over Earth history.

Postdepositional alteration can also impact $\delta^{34}\text{S}_{\text{pyrite}}$ records. For example, $\delta^{34}\text{S}_{\text{pyrite}}$ signatures can be variably overprinted during late-stage diagenesis if sulfide-bearing fluids migrate through strata that contain reactive iron. Based on distinctive morphology and major element geochemistry, separate populations of sedimentary pyrites can be distinguished, often with distinct $\delta^{34}\text{S}_{\text{pyrite}}$ characteristics (Fischer et al. 2014, Ono et al. 2008, Xiao et al. 2010). The ubiquity of late-stage sulfide mineralization (Hannington 2014) suggests that potential diagenetic overprinting of $\delta^{34}\text{S}_{\text{pyrite}}$ could be common.

LONG-TERM EVOLUTION OF SULFUR CYCLING: SEAWATER SULFATE ABUNDANCE

Today, marine sulfate concentrations are 28 mM, making sulfate the largest pool of oxidants within the oceans and second largest in Earth's exosphere, behind soil-hosted iron oxides (Hayes & Waldbauer 2006). Yet evidence from evaporite mineral sequences suggests that, on the early Earth, marine sulfate concentrations were much lower (<1 mM). Evaporation of modern ocean water results in the sequential precipitation of calcium carbonate (CaCO_3), followed by gypsum ($\text{CaSO}_4 \cdot 2\text{H}_2\text{O}$), followed by halite (NaCl). Archean (4.0–2.5 Ga) strata preserve records of evaporites that transition directly from carbonate to halite (Grotzinger & Kasting 1993); the absence of any sulfate evaporites in these strata suggests lower sulfate concentrations during the Archean. The first widespread bedded marine sulfate evaporites appear at ~ 1.2 Ga (Kah et al. 2001) and become commonplace in subsequent evaporitic strata, suggesting elevated sulfate levels (>2 mM) (Kah et al. 2004) in the ocean by the Mesoproterozoic (**Figure 7a**). However, the timing and magnitude of variations in sulfate concentration over the course of Earth history remain unknown. Reconstruction of these variations is a critical component to understanding the evolution of the global sulfur cycle as well as the redox budget of Earth's surface environment and the microbial assemblages it hosted over the course of Earth history.

Our best understanding of the evolution of the sulfate reservoir through time comes from chemical analysis of primary fluid inclusions in halite evaporites (**Figure 7a**). These inclusions retain (variably evaporated) seawater from their time of deposition and provide a direct window into ancient ocean chemistry. Original marine sulfate concentrations can be estimated by modeling the geochemical change to the fluids during evaporation (Brennan et al. 2004, Horita et al. 2002, Lowenstein et al. 2003, Timofeeff et al. 2006). The resulting records provide an estimate of sulfate concentrations throughout the Phanerozoic (**Figure 7a**).

Archean: con
from 4.0 to 2.5 Ga,
characterized by little
to no atmospheric
oxygen and abundant
dissolved iron (Fe^{2+})
in the oceans

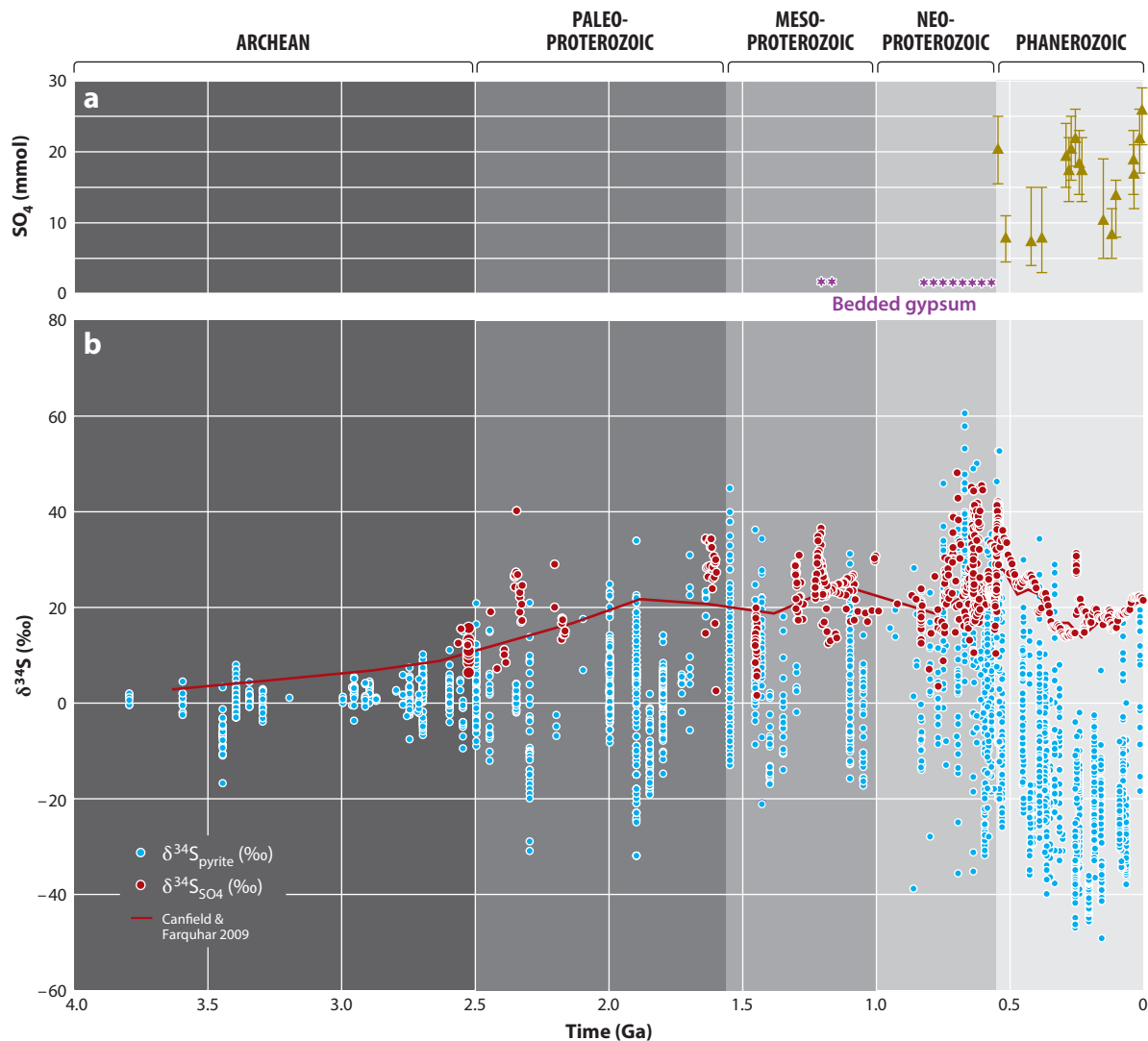


Figure 7

(a) Estimates of seawater sulfate based on the presence of gypsum evaporites in the Proterozoic and fluid inclusion data from Phanerozoic marine evaporites. (b) Compilation of sulfate and sulfide $\delta^{34}\text{S}$ records. After Canfield & Farquhar (2009). See the **Supplemental Material** for references; follow the **Supplemental Materials link** in the online version of this article or at <http://www.annualreviews.org/>.

Supplemental Material

Additional approaches have also been applied to further constrain sulfate concentrations. One method uses observed stratigraphic variability in $\delta^{34}\text{S}_{\text{CAS}}$ records to estimate sulfate concentrations (Kah et al. 2004). Although widely applied (Gill et al. 2007, 2011; Hurtgen et al. 2009; Loyd et al. 2012), these estimates are limited by our knowing neither the magnitude nor the origin of the forcing responsible for the observed $\delta^{34}\text{S}$ change; more critically, potential syndepositional or diagenetic alteration of the $\delta^{34}\text{S}_{\text{CAS}}$ signal could result in drastic underestimates of seawater sulfate concentrations. In a related approach, several authors have used lateral variability in $\delta^{34}\text{S}_{\text{CAS}}$

records as evidence for primary gradients in seawater $\delta^{34}\text{S}_{\text{SO}_4}$ and therefore for low sulfate concentrations (Hurtgen et al. 2006, Li et al. 2010). However, the low sulfate concentrations necessary to induce such large lateral gradients in water column $\delta^{34}\text{S}_{\text{SO}_4}$ may be at odds with large fractionations between coeval sulfate and pyrite in these strata. This approach may also be susceptible to local variations in $\delta^{34}\text{S}_{\text{CAS}}$ that arise during deposition, lithification, and/or diagenesis, rather than from primary variations in water column $\delta^{34}\text{S}_{\text{SO}_4}$. At this time, we do not have sufficient data to understand the scale and origin of lateral variability in $\delta^{34}\text{S}_{\text{CAS}}$ records. In sum, although there are several approaches to reconstruct seawater sulfate concentrations over time, the most conservative reconstructions come from the analysis of fluid inclusions in halite evaporites (**Figure 7a**).

LONG-TERM EVOLUTION OF SULFUR CYCLING: $\delta^{34}\text{S}$

Our understanding of the evolution of sulfur cycling over Earth history comes in large part from the records of sulfate and pyrite $\delta^{34}\text{S}$ from sedimentary strata. Several patterns emerge from these data, in both their means and their ranges, when viewed as a whole (**Figure 7b**). These are summarized briefly below, followed by a discussion of the main implications these data have for our understanding of the ancient sulfur cycle.

Seawater $\delta^{34}\text{S}_{\text{SO}_4}$ is thought to have been $\sim 0\%$ and relatively invariant during the Archean, although we have limited direct constraints (e.g., Guo et al. 2009, Paris et al. 2014b) prior to the appearance of the first bedded sulfate evaporites in the Mesoproterozoic (**Figure 7a**). The inference that Archean $\delta^{34}\text{S}_{\text{SO}_4}$ was $\sim 0\%$ is based on the relatively low variability of Archean $\delta^{34}\text{S}_{\text{pyrite}}$ ($\sim 0\%$; **Figure 7b**) and on the knowledge that pyrite was the predominant (if not exclusive) sink of sulfate from the oceans; together, these observations suggest that bulk $\delta^{34}\text{S}_{\text{pyrite}}$ should cluster around the $\delta^{34}\text{S}$ value of its parent sulfate. Beginning at approximately 2.4 Ga, there is an increase in the range of $\delta^{34}\text{S}_{\text{pyrite}}$ values (-25% to $+25\%$), with no change in mean value (**Figure 7b**). There are improved constraints on the evolution of $\delta^{34}\text{S}_{\text{SO}_4}$ in the Mesoproterozoic, where $\delta^{34}\text{S}_{\text{SO}_4}$ values have reached $\sim 20\%$ by 1.6 Ga and remain in this vicinity until ~ 600 Ma. Mean $\delta^{34}\text{S}_{\text{pyrite}}$ increases from 0% at ~ 1.5 Ga to $\sim 20\%$ at ~ 600 Ma. There is an increase in the $\delta^{34}\text{S}_{\text{pyrite}}$ range beginning at ~ 635 Ma and lasting through the late Cambrian (~ 500 Ma). This is associated with an increase in $\delta^{34}\text{S}_{\text{SO}_4}$ to $\sim 40\%$ at the Ediacaran–Cambrian boundary (~ 541 Ma) (**Figure 7b**). Throughout the early part of the Paleozoic $\delta^{34}\text{S}_{\text{SO}_4}$ values stay elevated (generally $\sim 30\%$), before beginning a decrease that continues until ~ 300 Ma, when $\delta^{34}\text{S}_{\text{SO}_4}$ reaches a minimum at $\sim 11\%$ (**Figure 7b**). In parallel, there is a decrease in mean $\delta^{34}\text{S}_{\text{pyrite}}$ from elevated values at the Ediacaran–Cambrian boundary until ~ 300 Ma. Beginning at ~ 300 Ma, $\delta^{34}\text{S}_{\text{SO}_4}$ values rise toward modern values of 21% with a parallel increase in mean $\delta^{34}\text{S}_{\text{pyrite}}$ values. The stratigraphic trends described above (**Figure 7b**) provide the basis for our understanding of the key elements in the evolution of the global sulfur cycle through time, discussed below.

There is significant scatter (~ 5 – 10%) in $\delta^{34}\text{S}_{\text{SO}_4}$ in many of these stratigraphic intervals (e.g., Jones & Fike 2013, Kampschulte & Strauss 2004). This variability is far larger than would be expected within an ocean that had an abundant sulfate reservoir (less than $\sim 1\%$)—and also far larger than typical analytical error ($\sim 0.3\%$). This additional scatter is likely the result of (syndepositional or diagenetic) alteration of $\delta^{34}\text{S}_{\text{SO}_4}$ signals—both from CAS and from sulfate evaporites. The origin of this variability needs to be better understood before we can have high confidence in our understanding of the evolution of the sulfur cycle during this period.

SECULAR VARIABILITY IN INPUTS: $\delta^{34}\text{S}_{\text{in}}$

The isotopic composition of sulfur entering the modern ocean ($\delta^{34}\text{S}_{\text{in}}$) is estimated to be 3% (Canfield 2004), representing a mixture of riverine inputs with $\delta^{34}\text{S}_{\text{in}} \sim 6\%$ and volcanic and

Cambrian: period from 541 to 488 Ma, marked by large biogeochemical changes leading to the Cambrian Explosion, a rapid increase in animal diversity

Ediacaran: period from 635 to 541 Ma, associated with increasing oxidation of the oceans and first appearance of bilaterian organisms

Neoproterozoic: era from 1,000 to 541 Ma, characterized by supercontinent breakup, global glaciations, and origins of basal metazoa

Proterozoic: eon from 2.5 to 0.541 Ga, characterized by a moderately oxidizing atmosphere and shallow ocean but reducing conditions in the deep ocean

hydrothermal inputs with $\delta^{34}\text{S}_{\text{in}} \sim 0\text{‰}$ (**Figure 4**). In the absence of significant biological fractionation, Archean $\delta^{34}\text{S}_{\text{in}}$ was likely $\sim 0\text{‰}$ (see above). However, if the existing records are representative of global sulfur cycling, mass balance considerations require that $\delta^{34}\text{S}_{\text{in}}$ must have been elevated relative to modern values throughout much of the intervening time, and particularly during the Ediacaran and Cambrian Periods (Canfield 2004, Fike & Grotzinger 2008). In a steady-state system—the preferred assumption of most long-term models of the sulfur cycle—the isotopic composition of sulfate entering the ocean must equal that of sulfur phases leaving the ocean. As there are two major sulfur sinks (sulfate and pyrite), $\delta^{34}\text{S}_{\text{in}}$ must lie between average $\delta^{34}\text{S}_{\text{SO}_4}$ and average $\delta^{34}\text{S}_{\text{pyrite}}$, equaling the weighted average of $\delta^{34}\text{S}_{\text{SO}_4}$ and $\delta^{34}\text{S}_{\text{pyrite}}$ buried. Yet, mean $\delta^{34}\text{S}_{\text{pyrite}}$ values from the interval between the start of the Neoproterozoic (1.0 Ga) and the end of the Cambrian (488 Ma) are well above 0‰ , reaching a maximum of $\sim 18\text{‰}$ during the Ediacaran Period (635–541 Ma) (Canfield 2004). These observations suggest that over Earth history $\delta^{34}\text{S}_{\text{in}}$ may have varied more than has previously been assumed, reaching values in excess of 12‰ during the latest Neoproterozoic—or that existing data have incompletely sampled the burial fluxes of reduced sulfur during these times, missing a substantial reservoir of ^{34}S -depleted sulfides.

Several possible mechanisms have been invoked to explain potential increases in $\delta^{34}\text{S}_{\text{in}}$. Long-term mechanisms to increase $\delta^{34}\text{S}_{\text{in}}$ involve either (a) the prolonged deep-sea burial and eventual subduction of ^{34}S -depleted pyrite, resulting in a corresponding increase in the $\delta^{34}\text{S}$ composition of the crustal sulfur reservoir (Canfield 2004), or (b) the preferential weathering of ^{34}S -enriched sulfates relative to ^{34}S -depleted pyrites under the lower-than-modern O_2 concentrations of the Proterozoic atmosphere (Fike & Grotzinger 2008). Both of these models were designed to explain the extensive interval (~ 1.5 Ga–500 Ma) of apparently elevated $\delta^{34}\text{S}_{\text{in}}$ and rely upon less oxidizing conditions during the Proterozoic relative to the Phanerozoic.

Additional, short-term changes in $\delta^{34}\text{S}_{\text{in}}$ and therefore in marine $\delta^{34}\text{S}_{\text{SO}_4}$ can also arise from changes in the weathering of sulfate evaporites (Halevy et al. 2012, Wortmann & Chernyavsky 2007, Wortmann & Paytan 2012). The fluxes associated with the formation and weathering of sulfate evaporites vary strongly through time, linked to changes in the areal extent of marine environments conducive to the formation and preservation of evaporites (Halevy et al. 2012). Dramatic changes in the flux of evaporites into (or out of) the ocean may result in rapid shifts in $\delta^{34}\text{S}_{\text{SO}_4}$ (Wortmann & Paytan 2012), shifts that can occur much faster than can be explained by steady-state mechanisms. Such rapid changes in the flux of evaporites (Wortmann & Chernyavsky 2007, Wortmann & Paytan 2012) are the likely cause for the rapid and well-resolved shifts in $\delta^{34}\text{S}_{\text{SO}_4}$ records from the Cretaceous and Cenozoic marine barites (Paytan et al. 1998, 2004)—records that have previously defied ready explanation (Kurtz et al. 2003).

LOW ϵ_{pyrite} DURING ARCHEAN SULFUR CYCLING

The Archean eon (4.0–2.5 Ga) is characterized by $\delta^{34}\text{S}$ records that suggest minimal fractionation between sulfate and sulfide (**Figure 7b**), although few data are available from the paired sulfate-sulfide samples necessary to constrain fractionation (Fike & Grotzinger 2008, Fike et al. 2006, Gill et al. 2011). Based on studies of the impact of sulfate concentration on fractionation during sulfate reduction, such limited $\delta^{34}\text{S}$ fractionation has been interpreted as evidence for sulfate abundances sufficiently low ($< 200 \mu\text{M}$) to inhibit fractionation during microbial sulfate reduction at this time (Habicht et al. 2002). Recent results (Crowe et al. 2014, Zhelezinskaia et al. 2014) have been interpreted to suggest even lower sulfate levels ($< 10 \mu\text{M}$) during the Archean.

However, high-resolution spatial analysis of Archean pyrites indicates that much higher fractionations were prevalent during the Archean than are apparent from bulk $\delta^{34}\text{S}_{\text{pyrite}}$ analyses

(Fischer et al. 2014, Kamber & Whitehouse 2007). These fractionations occur in pyrites that also contain the mass-independent signatures (e.g., $\delta^{33}\text{S}^3$) that are the hallmarks of Archean strata and are thought to derive from fractionation due to UV photochemistry prior to the accumulation of oxygen (and ozone) in the atmosphere at ~ 2.4 Ga (for a discussion of minor isotope behavior, see the review in Farquhar & Wing 2003). These data provide confidence that the large fractionations in $\delta^{34}\text{S}$ are primary and not the result of later-stage overprinting (Fischer et al. 2014, Kamber & Whitehouse 2007).

Abundant ferrous iron in the Archean acted as a near-quantitative sink for sulfide produced by sulfate reduction, where pyrite was the predominant sulfur sink from the ocean. These likely acted in concert to force bulk $\delta^{34}\text{S}_{\text{pyrite}}$ toward Archean seawater $\delta^{34}\text{S}_{\text{SO}_4}$ regardless of the actual magnitude of fractionation during microbial sulfur cycling. In strata younger than ~ 2.4 Ga, the range of fractionation between sulfate and bulk pyrite increases (**Figure 7b**). This offset could be due to increased sulfate concentrations no longer limiting the fractionation during microbial sulfate reduction or to a decrease in the efficiency of the pyrite sink associated with decreased iron availability (Fischer et al. 2014), highlighting how ambient iron availability can modulate the $\delta^{34}\text{S}$ signatures that get preserved in the sedimentary record.

INCREASING ϵ_{pyrite} THROUGH TIME

A further, gradual increase in maximum fractionation between sulfate and pyrite occurs during the late Neoproterozoic through the early Paleozoic. This increase in fractionation was attributed to an increase in the oxidative sulfur cycle and enhanced activity of microbial sulfur disproportionation (Canfield & Teske 1996), which can increase the isotopic fractionation between sulfate and sulfide (**Figure 3**). Such an interpretation agrees with previous suggestions of increased oxygenation at this time (Des Marais et al. 1992), as well as with subsequent reports (Canfield et al. 2007, Fike et al. 2006, Kaufman et al. 2007, Scott et al. 2008, Shields et al. 1997) arguing for increasing oxygenation during the Ediacaran Period (~ 635 – 541 Ma) (Bowring et al. 2007).

Role of Disproportionation

Insights into the potential role of disproportionation in the increase in fractionation between sulfate and sulfide at ~ 600 Ma can be gained from examining $\delta^{34}\text{S}$ records across chemoclines in modern marine environments, settings where the oxidative sulfur cycle and disproportionation would be anticipated to play important roles (Canfield & Teske 1996). However, in multiple cases, minima in isotopic fractionations between co-occurring sulfate and sulfide were found at the chemocline in a variety of environments. These observations include decreases in fractionation of ~ 10 – 20‰ approaching the chemocline within microbial mats from Guerrero Negro, Baja California, Mexico—a trend observed in multiple profiles, representing both day and night incubations and a range of sulfate concentrations (Fike et al. 2008, 2009). A similar-magnitude decrease in isotopic offsets between sulfate and sulfide was observed approaching the most oxidizing exterior portion of photosynthetic sulfur-cycling consortia of Sippewissett Salt Marsh, Massachusetts (Wilbanks et al. 2014). These “pink berries” consist of sulfate-reducing bacteria providing hydrogen sulfide to purple sulfur bacteria, which oxidize the sulfide to elemental sulfur and then to sulfate. A similar trend toward ^{34}S -enriched sulfide (and a minimum in sulfate-sulfide

$\Delta^{33}\text{S}$: a measure of mass-independent fractionation in ^{33}S relative to ^{32}S and ^{34}S ; nonzero values are diagnostic for Archean strata

$$^3\Delta^{33}\text{S} = 1,000 \times \left\{ \left(\frac{^{33}\text{S}/^{32}\text{S}}{^{33}\text{S}/^{32}\text{S}} \right)_{\text{sample}} / \left(\frac{^{33}\text{S}/^{32}\text{S}}{^{33}\text{S}/^{32}\text{S}} \right)_{\text{reference}} - \left[\left(\frac{^{34}\text{S}/^{32}\text{S}}{^{34}\text{S}/^{32}\text{S}} \right)_{\text{sample}} / \left(\frac{^{34}\text{S}/^{32}\text{S}}{^{34}\text{S}/^{32}\text{S}} \right)_{\text{reference}} \right]^{0.515} \right\}.$$

fractionation) is often found in the uppermost layers of modern sediments (Aller et al. 2008, 2010; Gao et al. 2013).

These observations all point toward a minimum in the isotopic difference between sulfate and sulfide at the chemocline, exactly where the oxidative sulfur cycle and disproportionation should be most pronounced (Canfield & Thamdrup 1996, Jørgensen & Postgate 1982). Yet, disproportionation should give rise to a maximum isotopic offset between sulfate and sulfide. Thus there is a disconnect between the observed difference in $\delta^{34}\text{S}$ between sulfate and sulfide at the chemocline and that expected if disproportionation were a major process impacting the isotopic offset between sulfate and sulfide. A focus of future work will involve using techniques of molecular microbiology to discern the links between active disproportionation and the generation of isotopic signatures in modern environments. This may be able to shed light on the environmental contribution of disproportionation to geological $\delta^{34}\text{S}$ signatures. The potential presence of sulfide oxidation (Zerkle et al. 2009) and/or disproportionation (Johnston et al. 2005a,b) during this time could also be assessed in these samples using the isotopic fractionation of minor sulfur isotopes.

Existing observations of $\delta^{34}\text{S}$ signatures (i.e., a minimum in sulfate-sulfide fractionation at the chemocline) preclude neither the presence nor the metabolic activity of disproportionating organisms in these modern environments. However, they do suggest that the impact of disproportionation on the sulfate-sulfide isotopic fractionation in these modern environments is negligible. It follows that it may be worthwhile to reexamine the impact of disproportionation on the $\delta^{34}\text{S}$ fractionation across the late Neoproterozoic–Paleozoic transition. If disproportionation is not the source of the ~ 600 Ma increase in apparent $\delta^{34}\text{S}$ fractionation between sulfate and sulfide, what other factors could be responsible?

Impact of Cell-Specific Sulfate Reduction Rate and Role of Electron Donors

Microbial sulfate reduction can result in large and variable $\delta^{34}\text{S}$ fractionation (0–66‰; see above). Based on our understanding of the importance of csSRR in regulating this isotopic fractionation today, secular changes in csSRR may have also modulated the observed fractionation between sulfate and pyrite $\delta^{34}\text{S}$ in the rock record (Habicht & Canfield 1996; Leavitt et al. 2013a; Sim et al. 2011a,b). For example, decreased average csSRR may have been responsible for the increased fractionation across the late Neoproterozoic–Paleozoic transition (**Figure 7b**). Similar arguments have been made invoking decreased csSRR to explain the increase in mean sulfate-pyrite fractionation from the Paleozoic into the Mesozoic (Leavitt et al. 2013a).

What environmental or ecological change could result in decreased csSRR moving into the Paleozoic? If reports of increasing oxygenation at this time are correct (Canfield et al. 2007, Fike et al. 2006, Kaufman et al. 2007, Scott et al. 2008, Shields et al. 1997), a decrease in csSRR may have resulted from increased aerobic respiration and more efficient degradation of organic matter within the water column and oxic upper portions of marine sediments at this time. Increased aerobic respiration would have resulted in a decrease in the amount of organic carbon available for use by sulfate-reducing microorganisms. The organic carbon that did make it to the zone of sulfate reduction would likely have also been more refractory (less easily utilized), as the more labile components of organic carbon would have been preferentially consumed in the overlying water column and oxic sediments. Thus, progressively decreasing csSRR over Earth history, associated with a general trend toward more oxidizing conditions (Holland 1973), may have had a role in regulating the range of $\delta^{34}\text{S}$ fractionation between sulfate and pyrite preserved in the geological record (**Figure 7b**), highlighting the coupling between the carbon and sulfur cycles over Earth history.

DYNAMIC CHANGES IN ϵ_{pyrite}

The rock record is replete with isotopic excursions in $\delta^{34}\text{S}_{\text{SO}_4}$ and/or $\delta^{34}\text{S}_{\text{pyrite}}$ (Fike & Grotzinger 2008; Fike et al. 2006; Gill et al. 2007; Gorjan et al. 2012; Hurtgen et al. 2006; Jones & Fike 2013; Kampschulte & Strauss 2004; Paytan et al. 1998, 2004). Most of these events have been interpreted to arise from changes in the relative burial flux of sulfur leaving the oceans as pyrite (f_{pyrite}), although changes to the flux and isotopic composition of sulfate delivered to the ocean have also been invoked (Canfield 2004, Fike & Grotzinger 2008, Halevy et al. 2012, Wortmann & Chernyavsky 2007, Wortmann & Paytan 2012). Changes in f_{pyrite} over Earth history are particularly important because they have direct implications for marine redox state and the accumulation of atmospheric oxygen. A change in pyrite burial (or in $\delta^{34}\text{S}_{\text{in}}$) would result in parallel, synchronous shifts in both seawater $\delta^{34}\text{S}_{\text{SO}_4}$ and globally averaged $\delta^{34}\text{S}_{\text{pyrite}}$, which occur on the (relatively slow) timescale of the response time of the marine sulfate reservoir (Kah et al. 2004), estimated to be ~ 13 Myr for modern sulfate concentrations and fluxes (Bernier 2001). In many cases, however, large-amplitude, stratigraphically coherent (i.e., not characterized by scatter) changes in $\delta^{34}\text{S}_{\text{pyrite}}$ are observed to occur faster than expected based on estimates of sulfate concentrations (**Figure 7a**) and inferred response times (Jones & Fike 2013). One interpretation of these data is that sulfate concentrations were lower at the time of deposition than many have previously assumed. An alternative explanation is that the excursions in $\delta^{34}\text{S}_{\text{pyrite}}$ may not have been driven by changes in pyrite burial. In many cases, paired $\delta^{34}\text{S}_{\text{CAS}}$ and $\delta^{34}\text{S}_{\text{pyrite}}$ data are not available through these excursions, and so independent constraints on the behavior of each proxy are lacking. As a consequence, unique solutions for possible causative mechanisms remain elusive.

One example for which paired $\delta^{34}\text{S}_{\text{CAS}}-\delta^{34}\text{S}_{\text{pyrite}}$ data are available comes from the end-Ordovician Hirnantian strata from Anticosti Island, Quebec, Canada. These strata were deposited during the Hirnantian Stage, at a time of characterized by glaciation (Desrochers et al. 2010, Finnegan et al. 2011) and associated mass extinctions and ecological perturbations (Copper 1999, Rohrssen et al. 2013). These carbonate ramp facies (Desrochers et al. 2010, Jones et al. 2011) preserve parallel 4‰ positive excursions in the stable isotope compositions of carbonate carbon ($\delta^{13}\text{C}_{\text{carbonate}}$) and organic carbon ($\delta^{13}\text{C}_{\text{organic}}$) (Jones et al. 2011, Long 1993), along with a positive 20‰ excursion in $\delta^{34}\text{S}_{\text{pyrite}}$, but no parallel excursion in $\delta^{34}\text{S}_{\text{CAS}}$ (Jones & Fike 2013). The absence of a parallel positive shift in $\delta^{34}\text{S}_{\text{CAS}}$ indicates that this excursion was not the result of an increase in pyrite burial (or $\delta^{34}\text{S}_{\text{in}}$). Instead, this $\delta^{34}\text{S}_{\text{pyrite}}$ excursion was interpreted to reflect a transient reduction in the biological fractionations associated with microbial sulfur cycling (ϵ_{pyrite}), due to differential organic carbon loading, sea level drawdown, and/or changing position of the chemocline within sediments during the glaciation (Jones & Fike 2013). Given the shallowing that occurs in these strata during the Hirnantian glaciation (Desrochers et al. 2010, Jones et al. 2011), and the increasing evidence that enhanced reworking and partial sulfide oxidation during shallowing can increase $\delta^{34}\text{S}_{\text{pyrite}}$ (Aller 2014, Aller et al. 2010, Gao et al. 2013), it is possible that the observed Hirnantian positive excursion in $\delta^{34}\text{S}_{\text{pyrite}}$ is a direct reflection of the changing depositional environment transitioning into and out of this glacial period. It is important to note that, although the proximal drivers of this $\delta^{34}\text{S}_{\text{pyrite}}$ excursion reflect changes in the local depositional environment, a $\delta^{34}\text{S}_{\text{pyrite}}$ excursion of similar magnitude is recorded in coeval Hirnantian strata across the globe (Gorjan et al. 2012, Wang et al. 1993, Yan et al. 2009). Thus, synchronous local changes across the globe are necessary to drive this excursion. Coordinated local environmental changes, such as changes in sea level (Desrochers et al. 2010, Jones et al. 2011), temperature (Finnegan et al. 2011), or respiration (Finnegan et al. 2012), might naturally arise associated with entering and exiting a glacial period. This record highlights the potential for large, globally correlative stratigraphic variations in $\delta^{34}\text{S}_{\text{pyrite}}$ to arise from coordinated local changes in the expression of isotopic fractionation during microbial sulfur cycling driven by ecological and/or environmental

changes that are rapid relative to the response time of the marine sulfate reservoir. Such dynamic behavior is not captured by standard steady-state treatment of the global sulfur cycle.

Superheavy pyrite:

pyrite with a $\delta^{34}\text{S}$ value higher than that of coexisting sulfates ($\delta^{34}\text{S}_{\text{pyrite}} > \delta^{34}\text{S}_{\text{CAS}}$)

SUPERHEAVY PYRITE

Throughout the $\delta^{34}\text{S}$ record, there are numerous examples where $\delta^{34}\text{S}_{\text{pyrite}}$ exceeds the value of coeval $\delta^{34}\text{S}_{\text{SO}_4}$ (**Figure 7b**). These so-called superheavy pyrites (Ries et al. 2009) are frequently associated with a high degree of stratigraphic variability and are particularly prevalent across the late Neoproterozoic–early Paleozoic transition.

No known microbial pathway is capable of generating sulfide that is enriched in ^{34}S relative to its parent sulfate. Therefore, the formation of such superheavy pyrites likely requires a multistep process. A plausible first step involves the generation of hydrogen sulfide with an isotopic composition similar to water column sulfate. This step could result either from minimal fractionation during sulfate reduction [e.g., caused by low (<0.2 mM) sulfate concentrations (Habicht et al. 2002, Ries et al. 2009)] or from Rayleigh-type distillation of a localized sulfate pool in pore waters giving rise to elevated sulfide $\delta^{34}\text{S}$. Either of these mechanisms could give rise to sulfide $\delta^{34}\text{S}$ that approaches $\delta^{34}\text{S}_{\text{SO}_4}$. A second process is then necessary in order to generate sulfide with $\delta^{34}\text{S}$ higher than that of coeval sulfate. The obvious candidate for this process is the partial oxidation of hydrogen sulfide. Abiotic oxidation of H_2S by O_2 has a kinetic fractionation of 5‰, resulting in an increase in $\delta^{34}\text{S}$ of the residual sulfide pool (Fry et al. 1988). This mechanism would allow for the generation of $\delta^{34}\text{S}_{\text{pyrite}}$ values enriched relative to seawater sulfate. Moreover, the partial oxidation of ^{34}S -depleted sulfide could decrease the $\delta^{34}\text{S}$ signature of the local sulfate pool. If this ^{34}S -depleted sulfate were incorporated into the preserved sulfate pool (e.g., as CAS in carbonate cements), it would act to artificially decrease the $\delta^{34}\text{S}_{\text{CAS}}$ signature and further increase the likelihood of superheavy pyrite formation.

The occurrence of superheavy pyrite has been used to argue for low seawater sulfate concentrations, particularly during the late Ediacaran (Ries et al. 2009). However, pyrites with $\delta^{34}\text{S}$ values in excess of seawater sulfate (+21‰) are found in many shallow-water environments today, particularly those characterized by oxidation during frequent sedimentary reworking (Aller et al. 2008, 2010; Gao et al. 2013), where the overlying seawater has ample sulfate (~28 mM). Examining the rock record reveals that many instances of superheavy pyrite are associated with shallow, high-energy depositional environments, like the Nama Group of Namibia (Grotzinger & Miller 2008, Saylor et al. 1995), where the samples described by Ries et al. (2009) originate. Together, these observations suggest that the occurrence of superheavy pyrite may relate primarily to the sedimentology of the local depositional environment rather than to ambient sulfate concentrations in seawater.

LOOKING FORWARD

Sedimentary strata are often composed of a complex mixture of allochthonous and autochthonous grains, muds, cements, and chemical precipitates, each with their own chemical signature and diagenetic histories. Our ability to extract the most relevant environmental information from ancient records of sulfate and pyrite $\delta^{34}\text{S}$ is often limited by our understanding of the depositional and diagenetic history of the samples—and by the tendency of traditional bulk analyses to average components that may possess distinct geochemical and isotopic signatures. Deciphering the multiple origins and histories of different sulfate- and sulfide-bearing phases in a sample is critical to extract meaningful information about its depositional and diagenetic environment. The field is moving toward coupled petrographic and geochemical analysis at ever-higher spatial resolution to identify and filter out the impact of syndepositional and diagenetic alteration on $\delta^{34}\text{S}$ records.

Parallel measurement of changes in abundance and isotopic composition of CAS can shed new light on how CAS is incorporated into carbonates and subsequently altered during lithification and diagenesis. Complementary approaches looking at the petrography, trace element geochemistry, and major and minor isotopic composition of different generations of pyrite and other metal sulfides can provide the same insights into the timing and conditions of formation of sulfides in the rock record. High-resolution (micrometer-scale) mapping of sulfur speciation using synchrotron-based X-ray spectromicroscopy is an exciting new approach to understand the spatial distribution of sulfur-bearing phases within complex sedimentary strata, allowing for the determination of CAS distributions among diverse carbonate phases and the identification of different generations of sulfides based on their trace element chemistry (Rose & Fike 2013).

Analytical techniques that can measure phase-specific $\delta^{34}\text{S}_{\text{CAS}}$ and $\delta^{34}\text{S}_{\text{pyrite}}$ values within a petrographic context are continually being refined. Although SIMS has a long history of providing insights into variability in sulfide $\delta^{34}\text{S}$ signals (Fike et al. 2008, 2009; Fischer et al. 2014; Kohn et al. 1998; Macfarlane & Shimizu 1991; Whitehouse et al. 2005; Williford et al. 2011; Winterholler et al. 2006; Xiao et al. 2010), promising new advances in $\delta^{34}\text{S}_{\text{CAS}}$ analysis make use of both SIMS techniques and multicollector inductively coupled plasma mass spectrometry (MC-ICP-MS). The SIMS approach has only moderate precision ($\delta^{34}\text{S}_{\text{CAS}} \sim 1\%$), but can analyze individual phases in a petrographic thin section with a spot size of 5–10 μm (Fike & Jones 2012). In contrast, the MC-ICP-MS approach (Paris et al. 2013, 2014a,b) offers unprecedented analytical precision [$\delta^{34}\text{S} \sim 0.1\%$ (2σ); $\delta^{33}\text{S} \sim 0.1\%$ (2σ)] on samples containing as little as 5–40 nmol S. Together, these microanalytical approaches, in complement to other isotope and elemental redox analyses, have the potential to identify the origin of spatial variability in $\delta^{34}\text{S}_{\text{CAS}}$ records, providing insights to screen data to create a high-fidelity record of the evolution of the global sulfur cycle over Earth history. New observations and techniques in biochemistry and molecular biology continue to provide better constraints on the sources of isotope fractionation during microbial sulfur transformations. As geochemists continue to develop novel high-resolution geochemical analyses, these in combination with other analytical approaches (e.g., $\delta^{18}\text{O}$ of sulfate) and phase- and mineral-specific analyses will provide new windows into the sulfur cycle of the ancient world.

SUMMARY POINTS

1. New observations coupling isotope geochemical and biochemical techniques provide constraints on the mechanisms and magnitudes of isotope fractionation during microbial sulfur transformations.
2. Depositional environments can have a strong impact on the abundance and isotopic composition of sulfur phases preserved in the rock record.
3. A large portion of variation in the sulfur cycle arises from non-steady-state behavior in the weathering of sulfate evaporites and in the expression of isotopic fractionation during microbial sulfur cycling.
4. Long-term evolution of fractionation during sulfur cycling could be driven primarily by the abundance and type of electron donors rather than by sulfate concentrations.
5. Small fractionations between sulfate and pyrite in the Archean may be a consequence of high iron abundance and efficient scavenging of sulfide to form pyrite in addition to low sulfate concentrations.
6. Regardless of its environmental significance, the role of disproportionation in creating the isotopic fractionation and variability preserved in the $\delta^{34}\text{S}$ record may be minor.

FUTURE ISSUES

1. The biochemical basis for, physiological controls on, and evolution of the machinery for generating isotopic fractionation during microbial sulfur cycling need better understanding. In particular, the isotope effects associated with individual enzymes are poorly constrained at present.
2. The mechanistic relationship between cell-specific sulfate reduction rates, environmental sulfate concentrations, and sulfur isotopic fractionation needs to be fully elucidated in order to understand the origin of and mechanism(s) responsible for changing fractionations observed in modern environments and preserved in the rock record.
3. Abiotic equilibrium and kinetic isotope fractionation factors between intermediate and reduced phases of sulfur need to be experimentally constrained.
4. We need to better understand how environmental and ecological conditions impact the generation of $\delta^{34}\text{S}$ signals—and their preservation in the sedimentary record.
5. Non-steady-state treatments of sulfur cycling need to be developed to account for rapid recycling of sedimentary evaporites and dynamic changes in microbial fractionation.
6. New analytical advances (MC-ICP-MS, SIMS, and synchrotron-based techniques) should be widely deployed to investigate the robustness and environmental dependence of $\delta^{34}\text{S}$ signals.

DISCLOSURE STATEMENT

The authors are not aware of any affiliations, memberships, funding, or financial holdings that might be perceived as affecting the objectivity of this review.

ACKNOWLEDGMENTS

This research was supported by National Science Foundation grants (EAR-0951509, OCE-1061476, EAR-1124389, and OCE-1155346), as well as a Packard Fellowship and a Hanse-Wissenschaftskolleg Fellowship to D.A.F. We thank Wil Leavitt and David Jones for discussions.

LITERATURE CITED

- Aller RC. 2014. Sedimentary diagenesis, depositional environments, and benthic fluxes. In *Treatise on Geochemistry*, Vol. 8: *The Oceans and Marine Geochemistry*, ed. MJ Mottl, H Elderfield, pp. 293–334. Amsterdam: Elsevier. 2nd ed.
- Aller RC, Blair NE, Brunskill GJ. 2008. Early diagenetic cycling, incineration, and burial of sedimentary organic carbon in the central Gulf of Papua (Papua New Guinea). *J. Geophys. Res.* 113:F01S09
- Aller RC, Madrid V, Chistoserdov A, Aller JY, Heilbrun C. 2010. Unsteady diagenetic processes and sulfur biogeochemistry in tropical deltaic muds: implications for oceanic isotope cycles and the sedimentary record. *Geochim. Cosmochim. Acta* 74:4671–92
- Amrani A, Said-Ahamed W, Lewan MD, Aizenshtat Z. 2006. Experiments on $\delta^{34}\text{S}$ mixing between organic and inorganic sulfur species during thermal maturation. *Geochim. Cosmochim. Acta* 70:5146–61
- Banner JL, Hanson GN. 1990. Calculation of simultaneous isotopic and trace element variations during water-rock interaction with applications to carbonate diagenesis. *Geochim. Cosmochim. Acta* 54:3123–37
- Berner RA. 1984. Sedimentary pyrite formation: an update. *Geochim. Cosmochim. Acta* 48:605–15

- Berner RA. 2001. Modeling atmospheric O₂ over Phanerozoic time. *Geochim. Cosmochim. Acta* 65:685–94
- Berner RA, Raiswell R. 1983. Burial of organic carbon and pyrite sulfur in sediments over Phanerozoic time: a new theory. *Geochim. Cosmochim. Acta* 47:855–62
- Boetius A, Ravenschlag K, Schubert CJ, Rickert D, Widdel F, et al. 2000. A marine microbial consortium apparently mediating anaerobic oxidation of methane. *Nature* 407:623–36
- Böttcher ME, Thamdrup B. 2001. Anaerobic sulfide oxidation and stable isotope fractionation associated with bacterial sulfur disproportionation in the presence of MnO₂. *Geochim. Cosmochim. Acta* 65:1573–81
- Böttcher ME, Thamdrup B, Vennemann TW. 2001. Oxygen and sulfur isotope fractionation during anaerobic bacterial disproportionation of elemental sulfur. *Geochim. Cosmochim. Acta* 65:1601–9
- Bowring SA, Grotzinger JP, Condon DJ, Ramezani J, Newall M. 2007. Geochronologic constraints on the chronostratigraphic framework of the Neoproterozoic Huqf Supergroup, Sultanate of Oman. *Am. J. Sci.* 307:1097–145
- Bradley AS, Leavitt WD, Johnston DT. 2011. Revisiting the dissimilatory sulfate reduction network. *Geobiology* 9:446–57
- Brand U, Veizer J. 1980. Chemical diagenesis of a multicomponent carbonate system. 1: Trace elements. *J. Sediment. Petrol.* 50:1219–36
- Brennan ST, Lowenstein TK, Horita J. 2004. Seawater chemistry and the advent of biocalcification. *Geology* 32:473–76
- Brunner B, Bernasconi SM. 2005. A revised isotope fractionation model for dissimilatory sulfate reduction in sulfate reducing bacteria. *Geochim. Cosmochim. Acta* 69:4759–71
- Bryant DA, Frigaard NU. 2006. Prokaryotic photosynthesis and phototrophy illuminated. *Trends Microbiol.* 14:488–96
- Burdett JW, Arthur MA, Richardson M. 1989. A Neogene seawater sulfate isotope age curve from calcareous pelagic microfossils. *Earth Planet. Sci. Lett.* 94:189–98
- Canfield DE. 1991. Sulfate reduction in deep-sea sediments. *Am. J. Sci.* 291:177–88
- Canfield DE. 2001a. Biogeochemistry of sulfur isotopes. *Rev. Mineral. Geochem.* 43:607–36
- Canfield DE. 2001b. Isotope fractionation by natural populations of sulfate-reducing bacteria. *Geochim. Cosmochim. Acta* 65:1117–24
- Canfield DE. 2004. The evolution of the Earth surface sulfur reservoir. *Am. J. Sci.* 304:839–61
- Canfield DE, Farquhar J. 2009. Animal evolution, bioturbation, and the sulfate concentration of the oceans. *PNAS* 106:8123–27
- Canfield DE, Farquhar J, Zerkle AL. 2010. High isotope fractionations during sulfate reduction in a low-sulfate euxinic ocean analog. *Geology* 38:415–18
- Canfield DE, Poulton SW, Narbonne GM. 2007. Late Neoproterozoic deep ocean oxygenation and the rise of animal life. *Science* 315:92–95
- Canfield DE, Teske A. 1996. Late Proterozoic rise in atmospheric oxygen concentration inferred from phylogenetic and sulphur-isotope studies. *Nature* 382:127–32
- Canfield DE, Thamdrup B. 1994. The production of ³⁴S-depleted sulfide during bacterial disproportionation of elemental sulfur. *Science* 266:1973–75
- Canfield DE, Thamdrup B. 1996. Fate of elemental sulfur in an intertidal sediment. *FEMS Microbiol. Ecol.* 19:95–103
- Chambers LA, Trudinger PA. 1975. Are thiosulfate and trithionate intermediates in dissimilatory sulfate reduction? *J. Bacteriol.* 123:36–40
- Chambers LA, Trudinger PA, Smith JW, Burns MS. 1975. Fractionation of sulfur isotopes by continuous cultures of *Desulfovibrio desulfuricans*. *Can. J. Microbiol.* 21:1602–7
- Claypool GE, Holser WT, Kaplan IR, Sakai H, Zak I. 1980. The age curves of sulfur and oxygen isotopes in marine sulfate and their mutual interpretation. *Chem. Geol.* 28:199–260
- Copper P. 1999. Brachiopods during and after the Late Ordovician mass extinctions on Anticosti Island, E Canada. *Acta Univ. Carol. Geol.* 43:207–9
- Crowe S, Paris G, Katsev S, Jones C, Kim ST, et al. 2014. Sulfate was a trace constituent of Archean seawater. *Science* 346:735–39
- Cypionka H. 1995. Solute transport and cell energetics. In *Sulfate-Reducing Bacteria*, ed. L. Barton, pp. 151–84. New York: Plenum

- Cypionka H. 2000. Oxygen respiration by *Desulfovibrio* species. *Annu. Rev. Microbiol.* 54:827–48
- Dahl C, Engels S, Pott-Sperling AS, Schulte A, Sander J, et al. 2005. Novel genes of the *dsr* gene cluster and evidence for close interaction of Dsr proteins during sulfur oxidation in the phototrophic sulfur bacterium *Allochromatium vinosum*. *J. Bacteriol.* 187:1392–404
- Des Marais DJ, Strauss H, Summons RE, Hayes JM. 1992. Carbon isotope evidence for the stepwise oxidation of the Proterozoic environment. *Nature* 359:605–9
- Desrochers A, Farley C, Achab A, Asselin E, Riva JF. 2010. A far-field record of the end Ordovician glaciation: the Ellis Bay Formation, Anticosti Island, Eastern Canada. *Palaeogeogr. Palaeoclimatol. Palaeoecol.* 296:248–63
- Drake J, Akagi J. 1977. Characterization of a novel thiosulfate-forming enzyme isolated from *Desulfovibrio vulgaris*. *J. Bacteriol.* 132:132–38
- Farquhar J, Wing B. 2003. Multiple sulfur isotopes and the evolution of the atmosphere. *Earth Planet. Sci. Lett.* 213:1–13**
- Fike DA, Finke N, Zha J, Blake G, Hoehler TM, Orphan VJ. 2009. The effect of sulfate concentration on (sub)millimeter-scale sulfide $\delta^{34}\text{S}$ in hypersaline cyanobacterial mats over the diurnal cycle. *Geochim. Cosmochim. Acta* 73:6187–204
- Fike DA, Gammon CL, Ziebis W, Orphan VJ. 2008. Micron-scale mapping of sulfur cycling across the oxycline of a cyanobacterial mat: a paired nanoSIMS and CARD-FISH approach. *ISME J.* 2:749–59
- Fike DA, Grotzinger JP. 2008. A paired sulfate–pyrite $\delta^{34}\text{S}$ approach to understanding the evolution of the Ediacaran–Cambrian sulfur cycle. *Geochim. Cosmochim. Acta* 72:2636–48
- Fike DA, Grotzinger JP. 2010. Reconstructing biogenic pyrite burial in evaporite basins: an example from the Ara Group, Sultanate of Oman. *Geology* 38:371–74
- Fike DA, Grotzinger JP, Pratt LM, Summons RE. 2006. Oxidation of the Ediacaran ocean. *Nature* 444:744–47
- Fike DA, Jones DS. 2012. *Micron-scale analysis of carbonate-associated sulfate by secondary ionization mass spectrometry: insights into spatial variability in $\delta^{34}\text{S}$* . Presented at AGU Fall Meet., Dec. 3–7, San Francisco. Abstr. B24E-05
- Finnegan S, Bergmann K, Eiler JM, Jones DS, Fike DA, et al. 2011. The magnitude and duration of Late Ordovician–Early Silurian glaciation. *Science* 331:903–6
- Finnegan S, Fike DA, Jones DS, Fischer WW. 2012. A temperature-dependent positive feedback on the magnitude of carbon isotope excursions. *Geosci. Can.* 39:122–31
- Finster K. 2008. Microbiological disproportionation of inorganic sulfur compounds. *J. Sulfur Chem.* 29:281–92
- Fischer WW, Fike DA, Johnson JE, Raub TD, Guan Y, Kirschvink JL. 2014. SQUID–SIMS is a useful approach to uncover primary signals in the Archean sulfur cycle. *PNAS* 111:5468–73
- Friedrich CG, Bardischewsky F, Rother D, Quentmeier A, Fischer J. 2005. Prokaryotic sulfur oxidation. *Curr. Opin. Microbiol.* 8:253–59
- Friedrich CG, Rother D, Bardischewsky F, Quentmeier A, Fischer J. 2001. Oxidation of reduced inorganic sulfur compounds by bacteria: emergence of a common mechanism? *Appl. Environ. Microbiol.* 67:2873–82
- Fry B, Gest H, Hayes JM. 1984. Isotope effects associated with the anaerobic oxidation of sulfide by the purple photosynthetic bacterium, *Chromatium vinosum*. *FEMS Microbiol. Lett.* 22:283–87
- Fry B, Gest H, Hayes JM. 1985. Isotope effects associated with the anaerobic oxidation of sulfite and thiosulfate by the photosynthetic bacterium *Chromatium vinosum*. *FEMS Microbiol. Lett.* 27:227–32
- Fry B, Ruf W, Gest H, Hayes JM. 1988. Sulfur isotope effects associated with oxidation of sulfide by O_2 in aqueous solution. *Chem. Geol.* 73:205–10
- Gao J, Fike DA, Aller RC. 2013. *Enriched pyrite $\delta^{34}\text{S}$ signals in modern tropical deltaic muds*. Presented at AGU Fall Meet., Dec. 9–13, San Francisco. Abstr. B31A-0352
- Garrels RM, Lerman A. 1981. Phanerozoic cycles of sedimentary carbon and sulfur. *PNAS* 78:4652–56
- Ghosh W, Dam B. 2009. Biochemistry and molecular biology of lithotrophic sulfur oxidation by taxonomically and ecologically diverse bacteria and archaea. *FEMS Microbiol. Rev.* 33:999–1043
- Gill BC, Lyons TW, Saltzman MR. 2007. Parallel, high-resolution carbon and sulfur isotope records of the evolving Paleozoic marine sulfur reservoir. *Palaeogeogr. Palaeoclimatol. Palaeoecol.* 256:156–73
- Gill BC, Lyons TW, Young SA, Kump LR, Knoll AH, Saltzman MR. 2011. Geochemical evidence for widespread euxinia in the Later Cambrian ocean. *Nature* 469:80–83

- Gomes ML, Hurtgen MT. 2013. Sulfur isotope systematics of a euxinic, low-sulfate lake: evaluating the importance of the reservoir effect in modern and ancient oceans. *Geology* 41:663–66
- Gorjan P, Kaiho K, Fike DA, Xu C. 2012. Carbon- and sulfur-isotope geochemistry of the Hirnantian (Late Ordovician) Wangjiawan (Riverside) section, South China: global correlation and environmental event interpretation. *Palaeogeogr. Palaeoclimatol. Palaeoecol.* 337–38:14–22
- Grotzinger JP, Kasting JF. 1993. New constraints on Precambrian ocean composition. *J. Geol.* 101:235–43
- Grotzinger JP, Miller R. 2008. The Nama Group. In *The Geology of Namibia*, ed. RM Miller, pp. 13229–72. Windhoek: Geol. Surv. Namib.
- Guo Q, Strauss H, Kaufman AJ, Schroeder S, Gutzmer J, et al. 2009. Reconstructing Earth's surface oxidation across the Archean–Proterozoic transition. *Geology* 37:399–402
- Habicht KS, Canfield DE. 1996. Sulphur isotope fractionation in modern microbial mats and the evolution of the sulphur cycle. *Nature* 382:342–43
- Habicht KS, Canfield DE. 1997. Sulfur isotope fractionation during bacterial sulfate reduction in organic-rich sediments. *Geochim. Cosmochim. Acta* 61:5351–61
- Habicht KS, Canfield DE, Rethmeier J. 1998. Sulfur isotope fractionation during bacterial reduction and disproportionation of thiosulfate and sulfite. *Geochim. Cosmochim. Acta* 62:2585–95
- Habicht KS, Gade M, Thamdrup B, Berg P, Canfield DE. 2002. Calibration of sulfate levels in the Archean ocean. *Science* 298:2372–74
- Halevy I, Peters SE, Fischer WW. 2012. Sulfate burial constraints on the Phanerozoic sulfur cycle. *Science* 337:331–34
- Hannington MD. 2014. Volcanogenic massive sulfide deposits. In *Treatise on Geochemistry*, Vol. 13: *Geochemistry of Mineral Deposits*, ed. SD Scott, pp. 463–88. Amsterdam: Elsevier. 2nd ed.
- Harrison A, Thode H. 1958. Mechanism of the bacterial reduction of sulphate from isotope fractionation studies. *Trans. Faraday Soc.* 54:84–92**
- Hauser LJ, Land ML, Brown SD, Larimer F, Keller KL, et al. 2011. Complete genome sequence and updated annotation of *Desulfovibrio alaskensis* G20. *J. Bacteriol.* 193:4268–69
- Hayes JM, Waldbauer JR. 2006. The carbon cycle and associated redox processes through time. *Philos. Trans. R. Soc. B* 361:931–50
- Hoehler TM, Alperin MJ, Albert DB, Martens CS. 1994. Field and laboratory studies of methane oxidation in an anoxic marine sediment: evidence for a methanogen-sulfate reducer consortium. *Glob. Biogeochem. Cycles* 8:451–63
- Holland HD. 1973. Systematics of isotopic composition of sulfur in oceans during the Phanerozoic and its implications for atmospheric oxygen. *Geochim. Cosmochim. Acta* 37:2605–16**
- Holser WT. 1977. Catastrophic chemical events in the history of the ocean. *Nature* 267:403–8**
- Horita J, Zimmermann H, Holland HD. 2002. Chemical evolution of seawater during the Phanerozoic: implications from the record of marine evaporites. *Geochim. Cosmochim. Acta* 66:3733–56
- Hurtgen MT, Halverson GP, Arthur MA, Hoffman PF. 2006. Sulfur cycling in the aftermath of a 635-Ma snowball glaciation: evidence for a syn-glacial sulfidic deep ocean. *Earth Planet. Sci. Lett.* 245:551–70
- Hurtgen MT, Pruss SB, Knoll AH. 2009. Evaluating the relationship between the carbon and sulfur cycles in the later Cambrian ocean: an example from the Port au Port Group, western Newfoundland, Canada. *Earth Planet. Sci. Lett.* 281:288–97
- Johnston DT. 2011. Multiple sulfur isotopes and the evolution of the Earth's surface sulfur cycle. *Earth Sci. Rev.* 106:161–83
- Johnston DT, Farquhar J, Wing BA, Kaufman AJ, Canfield DE, Habicht KS. 2005a. Multiple sulfur isotope fractionations in biological systems: a case study with sulfate reducers and sulfur disproportionators. *Am. J. Sci.* 305:645–60
- Johnston DT, Wing BA, Farquhar J, Kaufman AJ, Strauss H, et al. 2005b. Active microbial sulfur disproportionation in the Mesoproterozoic. *Science* 310:1477–79
- Jones DS, Fike DA. 2013. Dynamic sulfur and carbon cycling through the end-Ordovician extinction revealed by paired sulfate–pyrite $\delta^{34}\text{S}$. *Earth Planet. Sci. Lett.* 363:144–55
- Jones DS, Fike DA, Finnegan S, Fischer WW, Schrag DP, McCay D. 2011. Terminal Ordovician carbon isotope stratigraphy and glacioeustatic sea-level change across Anticosti Island (Québec, Canada). *Geol. Soc. Am. Bull.* 123:1645–64

The first detailed investigation into isotopic fractionation during microbial sulfate reduction.

The first attempt to quantitatively track sulfur fluxes using isotopes.

The generation of an early (evaporite-based) $\delta^{34}\text{S}_{\text{SO}_4}$ curve for the evolution of Phanerozoic seawater.

- Jørgensen BB. 1982. Mineralization of organic matter in the sea bed—the role of sulphate reduction. *Nature* 296:643–45
- Jørgensen BB, Postgate JR. 1982. Ecology of the bacteria of the sulfur cycle with special reference to anoxic–oxic interface environments. *Philos. Trans. R. Soc. B* 298:543–61
- Kah LC, Lyons TW, Chesley JT. 2001. Geochemistry of a 1.2 Ga carbonate–evaporite succession, northern Baffin and Bylot Islands: implications for Mesoproterozoic marine evolution. *Precambrian Res.* 111:203–34
- Kah LC, Lyons TW, Frank TD. 2004. Low marine sulphate and protracted oxygenation of the Proterozoic biosphere. *Nature* 431:834–38
- Kamber BS, Whitehouse MJ. 2007. Micro-scale sulphur isotope evidence for sulphur cycling in the late Archean shallow ocean. *Geobiology* 5:5–17
- Kampschulte A, Strauss H. 2004. The sulfur isotopic evolution of Phanerozoic seawater based on the analysis of structurally substituted sulfate in carbonates. *Chem. Geol.* 204:255–86
- Kaplan IR, Rittenberg SC. 1964. Microbiological fractionation of sulphur isotopes. *J. Gen. Microbiol.* 34:195–212**
- Kaufman AJ, Corsetti FA, Varni MA. 2007. The effect of rising atmospheric oxygen on carbon and sulfur isotope anomalies in the Neoproterozoic Johnnie Formation, Death Valley, USA. *Chem. Geol.* 237:47–63
- Kniemeyer O, Musat F, Sievert SM, Knittel K, Wilkes H, et al. 2007. Anaerobic oxidation of short-chain hydrocarbons by marine sulphate-reducing bacteria. *Nature* 449:898–901
- Knittel K, Boetius A. 2009. Anaerobic oxidation of methane: progress with an unknown process. *Annu. Rev. Microbiol.* 63:311–34
- Kobayashi K, Takahashi E, Ishimoto M. 1972. Biochemical studies on sulfate-reducing bacteria. XI. Purification and some properties of sulfite reductase, desulfoviridin. *J. Biochem.* 72:879–87
- Kohn MJ, Riciputi LR, Stakes D, Orange DL. 1998. Sulfur isotope variability in biogenic pyrite: reflections of heterogeneous bacterial colonization. *Am. Mineral.* 83:1454–68
- Kurtz AC, Kump LR, Arthur MA, Zachos JC, Paytan A. 2003. Early Cenozoic decoupling of the global carbon and sulfur cycles. *Paleoceanography* 18:1090
- Leavitt WD, Halevy I, Bradley AS, Johnston DT. 2013a. Influence of sulfate reduction rates on the Phanerozoic sulfur isotope record. *PNAS* 110:11244–49
- Leavitt WD, Pereira IC, Bradley AS, Guo W, Johnston DT. 2013b. Enzymatic constraints on the global S cycle: the fractionation factors of Dsr. *Mineral. Mag.* 77:1560 (Abstr.)
- Li C, Love GD, Lyons TW, Fike DA, Sessions AL, Chu X. 2010. A new stratified redox model for the Ediacaran ocean. *Science* 328:80–83
- Long DGF. 1993. Oxygen and carbon isotopes and event stratigraphy near the Ordovician–Silurian boundary, Anticosti Island, Québec. *Palaeogeogr. Palaeoclimatol. Palaeoecol.* 104:49–59
- Lowenstein TK, Hardie LA, Timofeeff MN, Demicco RV. 2003. Secular variation in seawater chemistry and the origin of calcium chloride basinal brines. *Geology* 31:857–60
- Lloyd SJ, Marengo PJ, Hagadorn JW, Lyons TW, Kaufman AJ, et al. 2012. Sustained low marine sulfate concentrations from the Neoproterozoic to the Cambrian: insights from carbonates of northwestern Mexico and eastern California. *Earth Planet. Sci. Lett.* 339–40:79–94
- Macfarlane AW, Shimizu N. 1991. SIMS measurements of $\delta^{34}\text{S}$ in sulfide minerals from adjacent vein and stratabound ores. *Geochim. Cosmochim. Acta* 55:525–41
- Michaels GB, Davidson JT, Peck HD. 1970. A flavin–sulfite adduct as an intermediate in the reaction catalyzed by adenylyl sulfate reductase from *Desulfovibrio vulgaris*. *Biochem. Biophys. Res. Commun.* 39:321–28
- Milucka J, Ferdelman TG, Polerecky L, Franzke D, Wegener G, et al. 2012. Zero-valent sulphur is a key intermediate in marine methane oxidation. *Nature* 491:541–46
- Nakagawa M, Ueno Y, Hattori S, Umemura M, Yagi A, et al. 2012. Seasonal change in microbial sulfur cycling in monomictic Lake Fukami-ike, Japan. *Limnol. Oceanogr.* 57:974–88
- Oliveira TF, Vornrhein C, Matias PM, Venceslau SS, Pereira IAC, Archer M. 2008. The crystal structure of *Desulfovibrio vulgaris* dissimilatory sulfite reductase bound to DsrC provides novel insights into the mechanism of sulfate respiration. *J. Biol. Chem.* 283:34141–49
- Ono S, Beukes NJ, Rumble D. 2008. Origin of two distinct multiple-sulfur isotope compositions of pyrite in the 2.5 Ga Klein Naute Formation, Griqualand West Basin, South Africa. *Precambrian Res.* 169:48–57

- Orphan VJ, House CH, Hinrichs KU, McKeegan KD, DeLong EF. 2001. Methane-consuming archaea revealed by directly coupled isotopic and phylogenetic analysis. *Science* 293:484–87
- Paris G, Adkins JF, Sessions AL, Webb SM, Fischer WW. 2014a. Neoproterozoic carbonate-associated sulfate records positive $\delta^{33}\text{S}$ anomalies. *Science* 346:739–41
- Paris G, Fehrenbacher JS, Sessions AL, Spero HJ, Adkins JF. 2014b. Experimental determination of carbonate-associated sulfate $\delta^{34}\text{S}$ in planktonic foraminifera shells. *Geochem. Geophys. Geosyst.* 15:1452–61
- Paris G, Sessions AL, Subhas AV, Adkins JF. 2013. MC-ICP-MS measurement of $\delta^{33}\text{S}$ and $\delta^{34}\text{S}$ in small amounts of dissolved sulfate. *Chem. Geol.* 345:50–61
- Parnell J, Boyce AJ, Mark D, Bowden SA, Spinks S. 2010. Early oxygenation of the terrestrial environment during the Mesoproterozoic. *Nature* 468:290–93
- Paytan A, Kastner M, Campbell D, Thiemens MH. 1998. Sulfur isotopic composition of Cenozoic seawater sulfate. *Science* 282:1459–62
- Paytan A, Kastner M, Campbell D, Thiemens MH. 2004. Seawater sulfur isotope fluctuations in the Cretaceous. *Science* 304:1663–65
- Paytan A, Mearon S, Cobb K, Kastner M. 2002. Origin of marine barite deposits: Sr and S isotope characterization. *Geology* 30:747–50
- Peck H. 1962. Comparative metabolism of inorganic sulfur compounds in microorganisms. *Bacteriol. Rev.* 26:67–94
- Philippot P, Van Zuilen M, Lepot K, Thomazo C, Farquhar J, Van Kranendonk MJ. 2007. Early Archaeal microorganisms preferred elemental sulfur, not sulfate. *Science* 317:1534–37
- Raab M, Spiro B. 1991. Sulfur isotopic variations during seawater evaporation with fractional crystallization. *Chem. Geol.* 86:323–33
- Rabus R, Hansen TA, Widdel F. 2013. Dissimilatory sulfate- and sulfur-reducing prokaryotes. In *The Prokaryotes: Prokaryotic Physiology and Biochemistry*, ed. E Rosenberg, EF DeLong, E Stackenbrandt, S Lory, F Thompson, pp. 309–404. Berlin: Springer-Verlag
- Raven MR, Adkins JF, Werne JP, Lyons TW, Sessions AL. 2015. Sulfur isotopic composition of individual organic compounds from Cariaco Basin sediments. *Org. Geochem.* 80:53–59
- Rees CE. 1973. Steady-state model for sulfur isotope fractionation in bacterial reduction processes. *Geochim. Cosmochim. Acta* 37:1141–62
- Rickard D. 1995. Kinetics of FeS precipitation. Part 1: Competing reaction mechanisms. *Geochim. Cosmochim. Acta* 59:4367–79
- Rickard D, Luther GW. 1997. Kinetics of pyrite formation by the H_2S oxidation of iron (II) monosulfide in aqueous solutions between 25 and 125°C: the mechanism. *Geochim. Cosmochim. Acta* 61:135–47
- Ries JB, Fike DA, Pratt LM, Lyons TW, Grotzinger JP. 2009. Super-heavy pyrite ($\delta^{34}\text{S}_{\text{pyr}} > \delta^{34}\text{S}_{\text{CAS}}$) in the terminal Proterozoic Nama Group, Southern Namibia: a consequence of low seawater sulfate at the dawn of animal life. *Geology* 37:743–46
- Rohrsen M, Love GD, Fischer WW, Finnegan S, Fike DA. 2013. Lipid biomarkers record fundamental changes in the microbial community structure of tropical seas during the Late Ordovician Hirnantian glaciation. *Geology* 41:127–30
- Rose CV, Fike DA. 2013. *Deciphering Earth history: mapping the spatial distribution and speciation of sulfur in Ordovician carbonates*. Presented at Midwest Geobiol. Symp., Sept. 28, Indianapolis, IN
- Sass H, Steuber J, Kroder M, Kroneck P, Cypionka H. 1992. Formation of thionates by fresh-water and marine strains of sulfate-reducing bacteria. *Arch. Microbiol.* 158:418–21
- Saylor BZ, Grotzinger JP, Germs GJB. 1995. Sequence stratigraphy and sedimentology of the Neoproterozoic Kuibis and Schwarzrand Subgroups (Nama Group), Southwestern Namibia. *Precambrian Res.* 73:153–71
- Scott C, Lyons TW, Bekker A, Shen Y, Poulton SW, et al. 2008. Tracing stepwise oxygenation of the Proterozoic biosphere. *Nature* 452:456–59
- Shen Y, Buick R, Canfield DE. 2001. Isotopic evidence for microbial sulfate reduction in the early Archean era. *Nature* 410:77–81
- Shields G, Stille P, Brasier MD, Atudorei NV. 1997. Stratified oceans and oxygenation of the late Precambrian environment: a postglacial geochemical record from the Neoproterozoic of W Mongolia. *Terra Nova* 9:218–22

A summary of our best current understanding of how sulfate reduction works at the biochemical level.

- Sim MS, Bosak T, Ono S. 2011a. Large sulfur isotope fractionation does not require disproportionation. *Science* 333:74–77
- Sim MS, Ono S, Bosak T. 2012. Effects of iron and nitrogen limitation on sulfur isotope fractionation during microbial sulfate reduction. *Appl. Environ. Microbiol.* 78:8368–76
- Sim MS, Ono S, Donovan K, Templer SP, Bosak T. 2011b. Effect of electron donors on the fractionation of sulfur isotopes by a marine *Desulfovibrio* sp. *Geochim. Cosmochim. Acta* 75:4244–59
- Staudt WJ, Reeder RJ, Schoonen MAA. 1994. Surface structural controls on compositional zoning of SO_4^{2-} and SeO_4^{2-} in synthetic calcite single crystals. *Geochim. Cosmochim. Acta* 58:2087–98
- Staudt WJ, Schoonen MAA. 1995. Sulfate incorporation into sedimentary carbonates. *ACS Symp. Ser.* 612:332–45
- Strauss H. 1997. The isotopic composition of sedimentary sulfur through time. *Palaeogeogr. Palaeoclimatol. Palaeoecol.* 132:97–118
- Takano B. 1995. Geochemical implications of sulfate in sedimentary carbonates. *Chem. Geol.* 49:393–403
- Tarpgaard IH, Røy H, Jørgensen BB. 2011. Concurrent low- and high-affinity sulfate reduction kinetics in marine sediment. *Geochim. Cosmochim. Acta* 75:2997–3010
- Timofeeff MN, Lowenstein TK, da Silva MAM, Harris NB. 2006. Secular variation in the major-ion chemistry of seawater: evidence from fluid inclusions in Cretaceous halites. *Geochim. Cosmochim. Acta* 70:1977–94
- Troelsen H, Jørgensen BB. 1982. Seasonal dynamics of elemental sulfur in two coastal sediments. *Estuar. Coast. Shelf Sci.* 15:255–66
- Venceslau SS, Stockdreher Y, Dahl C, Pereira IAC. 2014. The “bacterial heterodisulfide” DsrC is a key protein in dissimilatory sulfur metabolism. *Biochim. Biophys. Acta* 1837:1148–64**
- Visscher PT, Reid RP, Bebout BM. 2000. Microscale observations of sulfate reduction: correlation of microbial activity with lithified micritic laminae in modern marine stromatolites. *Geology* 28:919–22
- Wang K, Orth CJ, Atrep M, Chatterton BDE, Wang X, Li JJ. 1993. The great latest Ordovician extinction on the South China Plate: chemostratigraphic studies of the Ordovician-Silurian boundary interval on the Yangtze Platform. *Palaeogeogr. Palaeoclimatol. Palaeoecol.* 104:61–79
- Whitehouse MJ, Kamber BS, Fedo CM, Lepland A. 2005. Integrated Pb- and S-isotope investigation of sulphide minerals from the early Archaean of southwest Greenland. *Chem. Geol.* 222:112–31
- Wilbanks EG, Jaekel U, Salman V, Humphrey PT, Eisen JA, et al. 2014. Microscale sulfur cycling in the phototrophic pink berry consortia of the Sippewissett Salt Marsh. *Environ. Microbiol.* 16:3398–415
- Williford KH, Van Kranendonk MJ, Ushikubo T, Kozdon R, Valley JW. 2011. Constraining atmospheric oxygen and seawater sulfate concentrations during Paleoproterozoic glaciation: in situ sulfur three-isotope microanalysis of pyrite from the Turee Creek Group, Western Australia. *Geochim. Cosmochim. Acta* 75:5686–705
- Wing BA, Halevy I. 2014. Intracellular metabolite levels shape sulfur isotope fractionation during microbial sulfate respiration. *PNAS* 111:18116–25
- Winterholler B, Hoppe P, Andreae MO, Foley S. 2006. Measurement of sulfur isotope ratios in micrometer-sized samples by NanoSIMS. *Appl. Surf. Sci.* 252:7128–31
- Wortmann UG, Chernyavsky BM. 2007. Effect of evaporite deposition on Early Cretaceous carbon and sulphur cycling. *Nature* 446:654–56
- Wortmann UG, Paytan A. 2012. Rapid variability of seawater chemistry over the past 130 million years. *Science* 337:334–36
- Xiao S, Schiffbauer JD, McFadden KA, Hunter J. 2010. Petrographic and SIMS pyrite sulfur isotope analyses of Ediacaran chert nodules: implications for microbial processes in pyrite rim formation, silicification, and exceptional fossil preservation. *Earth Planet. Sci. Lett.* 297:481–95
- Yan D, Chen D, Wang Q, Wang J, Wang Z. 2009. Carbon and sulfur isotopic anomalies across the Ordovician–Silurian boundary on the Yangtze Platform, South China. *Palaeogeogr. Palaeoclimatol. Palaeoecol.* 297:32–39
- Zerkle AL, Farquhar J, Johnston DT, Cox RP, Canfield DE. 2009. Fractionation of multiple sulfur isotopes during phototrophic oxidation of sulfide and elemental sulfur by a green sulfur bacterium. *Geochim. Cosmochim. Acta* 73:291–306
- Zhelezinskaia I, Kaufman AJ, Farquhar J, Cliff J. 2014. Large sulfur isotope fractionations associated with Neoproterozoic microbial sulfate reduction. *Science* 346:742–44



Contents

A Conversation with James J. Morgan <i>James J. Morgan and Dianne K. Newman</i>	1
Global Monsoon Dynamics and Climate Change <i>An Zhibeng, Wu Guoxiong, Li Jianping, Sun Youbin, Liu Yimin, Zhou Weijian, Cai Yanjun, Duan Anmin, Li Li, Mao Jianguyu, Cheng Hai, Shi Zhennguo, Tan Liangcheng, Yan Hong, Ao Hong, Chang Hong, and Feng Juan</i>	29
Conservation Paleobiology: Leveraging Knowledge of the Past to Inform Conservation and Restoration <i>Gregory P. Dietl, Susan M. Kidwell, Mark Brenner, David A. Burney, Karl W. Flessa, Stephen T. Jackson, and Paul L. Koch</i>	79
Jadeitites and Plate Tectonics <i>George E. Harlow, Tatsuki Tsujimori, and Sorena S. Sorensen</i>	105
Macroevolutionary History of the Planktic Foraminifera <i>Andrew J. Fraass, D. Clay Kelly, and Shanan E. Peters</i>	139
Continental Lower Crust <i>Bradley R. Hacker, Peter B. Kelemen, and Mark D. Behn</i>	167
Oceanic Forcing of Ice-Sheet Retreat: West Antarctica and More <i>Richard B. Alley, Sridhar Anandakrishnan, Knut Christianson, Huw J. Horgan, Atsu Muto, Byron R. Parizek, David Pollard, and Ryan T. Walker</i>	207
From Geodetic Imaging of Seismic and Aseismic Fault Slip to Dynamic Modeling of the Seismic Cycle <i>Jean-Philippe Avouac</i>	233
The Pyrogenic Carbon Cycle <i>Michael I. Bird, Jonathan G. Wynn, Gustavo Saiz, Christopher M. Wurster, and Anna McBeath</i>	273
The Architecture, Chemistry, and Evolution of Continental Magmatic Arcs <i>Mihai N. Ducea, Jason B. Saleeby, and George Bergantz</i>	299
Paleosols as Indicators of Paleoenvironment and Paleoclimate <i>Neil J. Tabor and Timothy S. Myers</i>	333

Role of Arc Processes in the Formation of Continental Crust <i>Oliver Jagoutz and Peter B. Kelemen</i>	363
Environment and Climate of Early Human Evolution <i>Naomi E. Levin</i>	405
Magma Fragmentation <i>Helge M. Gonnermann</i>	431
Atmospheric Escape from Solar System Terrestrial Planets and Exoplanets <i>Feng Tian</i>	459
A Tale of Amalgamation of Three Permo-Triassic Collage Systems in Central Asia: Oroclines, Sutures, and Terminal Accretion <i>Wenjiao Xiao, Brian F. Windley, Shu Sun, Jiliang Li, Baochun Huang, Chunming Han, Chao Yuan, Min Sun, and Hanlin Chen</i>	477
Atmospheric Dynamics of Hot Exoplanets <i>Kevin Heng and Adam P. Showman</i>	509
Transient Creep and Strain Energy Dissipation: An Experimental Perspective <i>Ulrich Faul and Ian Jackson</i>	541
Rapid Plate Motion Variations Through Geological Time: Observations Serving Geodynamic Interpretation <i>Giampiero Iaffaldano and Hans-Peter Bunge</i>	571
Rethinking the Ancient Sulfur Cycle <i>David A. Fike, Alexander S. Bradley, and Catherine V. Rose</i>	593
Indexes	
Cumulative Index of Contributing Authors, Volumes 34–43	623
Cumulative Index of Article Titles, Volumes 34–43	628

Errata

An online log of corrections to *Annual Review of Earth and Planetary Sciences* articles may be found at <http://www.annualreviews.org/errata/earth>